DYNAMICS OF CROSS-SHORE THERMAL EXCHANGE

ON A TROPICAL FORE-REEF

A THESIS SUBIMTTED TO THE GRADUATE DIVISION OF THE UNIVERSITY OF HAWAI`I AT MĀNOA IN PARTIAL FULFILLMENT OF THE REQUIREMENTS FOR THE DEFGREE OF

MASTER OF SCIENCE

IN

OCEAN AND RESOURCES ENGINEERING

MAY 2012

By:

Lauren Tuthill

Thesis Committee:

Geno Pawlak, Chairperson
Mark Merrifield
Eva-Marie Nosal

Acknowledgements

The work presented here was carried out with support from NSF project OCE-0824832. The author also received support from the City and County of Honolulu via a collaborative project with Sea Engineering, Inc.

Abstract

The dynamics of cross-shelf circulation influence the exchange of water masses and the distribution of heat, salt, nutrients, contaminants, sediment, and planktonic organisms like larvae or phytoplankton in the nearshore coastal ocean. In addition, in the case of coral reefs, the horizontal redistribution of heat by cross-shelf circulation can moderate the daily variations in temperature experienced by polyps, thus potentially reducing thermal stress. Observations of the velocity structure at the Kilo Nalu Observatory on the south shore of Oahu, Hawaii show that thermally driven baroclinic exchange is the dominant mechanism for cross-shore transport for this tropical forereef environment. Estimates of the exchange and net fluxes show that the average residence time for the zone shoreward of the 12m isobath is generally less than one day. The thermal forcing is identified from the relationship between the magnitude of the exchange and the surface heat flux. Temporal variability of the exchange is examined and compared with meteorological data and water properties. Dynamic flow regimes are characterized following the framework presented by Monismith et al. 2006, and the observations at Kilo Nalu are shown to be in the unsteady temperature regime. Spatial observations are presented which support our observations of the thermally driven exchange, but also illustrate the complexity associated with alongshore variability.

Table of Contents

Acknowledgements ii
Abstract iii
List of Tables v
List of Figures vi
Chapter 1. Dynamics of Cross-shore Thermal Exchange at the Kilo Nalu Observatory ... 1
1. Introduction 1
2. Background 2
3. Methods & Observations 4
4. Results and Discussion 5
4.1. Depth Averaged and Exchange Flow 5
4.2. Potential driving mechanisms of exchange 9
4.3. Temporal Variability 14
4.4. Dynamics of thermally driven exchange 17
5. Conclusions 19
Chapter 2. Spatial Variability Affecting Cross-shore Thermal Exchange at Kilo Nalu ... 20
1. Introduction 20
2. Experimental Design 20
3. Observations 22
3.1. Background Conditions 22
3.2. Ala Moana Reef 24
3.3. Offshore Ala Moana 25
3.4. Ala Moana Lagoon 27
3.5. Ala Moana Profiles 29
4. Discussion and Conclusions 29
References 32

List of Tables

1.1. Six regimes as described by Monismith et al. (2006)..3

2.1. List of instrumentation used and data collected..22

List of Figures

1.1. Idealized wedge representing the volume inshore of the Kilo Nalu site. 2

1.2. Map of Kilo Nalu and surrounding area 5

1.3. Comparison of depth averaged velocities to the average velocity magnitude 6

1.4. Diurnal average of cross-shore current and temperature profiles from 2010. 6

1.5. Spectra of cross- and along-shore currents 7

1.6. Tides, along- and cross-shore velocity profiles 8

1.7. Exchange and net volume flux approximated for Kilo Nalu 8

1.8. EOF modes 1 and 2 10

1.9. Diurnal composite for EOF mode 1 10

1.10. EOF mode 1 2010 time series 11

1.11. Average heating and cooling profiles 11

1.12. Diurnal composite for cross-shore velocity shear 12

1.13. Advective heat flux diurnal composite, correlation, and time series 12

1.14. Environmental conditions during May 18-28, 2010 15

1.15. Environmental conditions during a Kona storm, February 2-3, 2010 16

1.16. Relation of advective heat flux, V, to u_f and $u_f{}^3/u_*$ 18

2.1. Map of south shore Oahu and experimental setup 21

2.2. Bathymetry of south shore Oahu 22

2.3. Environmental conditions April 27 – May 6, 2011 23

2.4. Water temperature on Ala Moana reef and Honolulu Harbor 25

2.5. REMUS track distance 25

2.6. REMUS temperature and salinity profiles and transects 26

2.7 REMUS measurements of temperature and salinity 26

2.8. Depth-averaged along- and cross-shore currents 27

2.9. Ala Moana lagoon measurements of temperature and salinity 28

2.10. Ala Moana lagoon measurements averages of temperature and salinity 28

2.11. Contour plots of temperature and density in Ala Moana lagoon 29

2.12. Temperature, salinity, and density profiles 30

Chapter 1. Dynamics of Cross-shore Thermal Exchange at the Kilo Nalu Observatory

1. Introduction

Nearshore hydrodynamics affect the transport of nutrients, organisms, heat and salt, which are vital to the health of ecosystems such as coral reefs. Habitat dynamics, including rates of larval dispersion and recruitment, are regulated by the physical processes over the reef and the degree of hydrodynamic closure between adjacent systems (Hatcher, 1997; Cowen and Sponaugle, 2009). Cross-shelf fluxes are especially critical to the import of phytoplankton and nutrients and the export of wastes. It has been observed that the rate of nearshore flushing affects the balance between grazing and recycling of organic matter (Genin et al. 2009, Hatcher, 1997). At the Kilo Nalu Observatory on the south shore of Oahu, Hawaii, the cross-isobath flow is vital not only to the reef itself, but also to the nearshore water quality for this densely populated area (Paul et al. 1997, Kellogg et al. 1995).

The mechanisms that drive cross-shore flow are numerous and depend greatly on shelf width, bathymetry, and stratification. On continental shelves, along-shore winds drive upwelling and Ekman transport on the mid and outer shelf regions (Huyer, 1976). Symonds and Gardiner-Garden (1994) have more recently shown that buoyancy driven currents can drive cross-shelf exchange, such as on the southeastern coast of Australia. On inner continental shelves, Fewings et al. (2008) found that cross-shelf winds are the main forcing mechanism of the cross-shelf currents, driving a two layer exchange. Waves and stratification were of secondary importance, regulating the strength and structure of the velocity profile. Other studies have shown that surface waves are important in driving mean flow (Hench et al. 2008) and Stokes drift (Monismith and Fong, 2004) for nearshore coastal circulation. Internal tidal bores, which bring in colder, saltier water from offshore waters, can play an important role in regulating temperature over a reef as well as bringing dissolved and suspended materials up from subthermocline waters (Leichter et al. 1996).

Buoyancy driven circulation has also been studied around atolls (e.g. Boden, 1952), in the Red Sea (Phillips, 1966), on continental shelves (Symonds and Gardiner-Garden, 1994), and over a fringing reef (Monismith et al. 2006). Observations and models have shown that due to surface cooling, cold waters sink and flow offshore and are compensated by an onshore flow at the surface. We present observations that suggest that such thermally driven flows are the main driving mechanism of the cross-shore currents at Kilo Nalu. Kilo Nalu is located in a fringing reef between the popular beaches of Ala Moana and Waikiki and the industrial port at Honolulu Harbor. Previous research has shown that the currents in this area are mainly regulated by an M2 tide that flows along-isobath (Pawlak et al. 2009). This paper presents evidence that the weaker cross-shore currents are dominated by a thermally driven baroclinic exchange flow.

2. Background

In order to study the thermally driven baroclinic exchange flow, the physical problem can be idealized as a two-dimensional wedge with unit width (Figure 1). As heat flux is applied uniformly to the surface, shallower waters heat and cool more rapidly than the deeper waters. Thus, in the cross-shore direction, a temperature gradient is set up due to the change in depth. During cooling, denser water generated at the surface sinks and flows offshore, and is compensated by a return flow at the surface. The opposite occurs during heating when warmer surface water flows offshore, compensated by an onshore flow at depth. The mechanics of this exchange flow are governed by the momentum and thermal energy balance equations. Following the work of Monismith et al. (2006), the problem can be simplified by examining various dynamic limits. The two-dimensional cross-shore horizontal momentum equation for a non-rotating fluid is given by

$$\frac{\partial V}{\partial t} + V\frac{\partial V}{\partial y} + W\frac{\partial V}{\partial z} = -\frac{1}{\rho_o}\frac{\partial P}{\partial y} + \frac{\partial}{\partial z}\left(\nu_t \frac{\partial V}{\partial z}\right) \tag{1}$$

where V and W are the horizontal and vertical velocity components respectively, P is pressure, and ρ_o is the reference density of water (1000 kg m^{-3}). The turbulent eddy viscosity, ν_t, is scaled as qD, where D is the total water depth and q is the relevant turbulent velocity scale, which for our case is the friction velocity, u_*, associated with the longshore current, neglecting surface stress. For the momentum balance, the pressure gradient must be offset by some combination of advection, mixing, and an unsteady inertial flow. To simplify the problem, three separate dynamic limits can be considered:

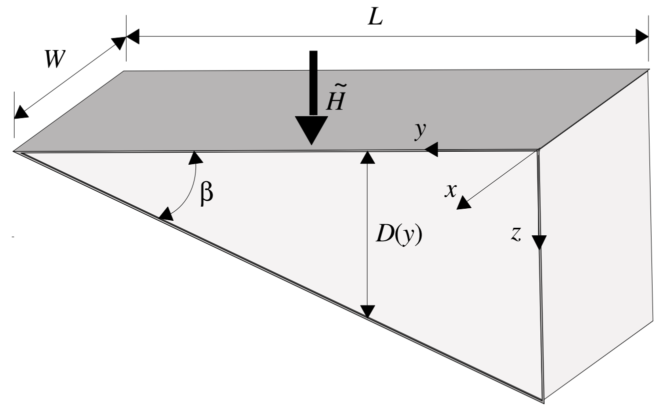

Figure 1. Idealized wedge representing the volume inshore of the Kilo Nalu site. Currents are positive onshore and surface heat flux is positive when heating. Depth changes as a function of y, distance on/offshore.

$$\left.\begin{array}{lll} \text{1) Unsteady inertia} & \dfrac{\partial V}{\partial t} \sim \dfrac{1}{\rho_o}\dfrac{\partial P}{\partial y} \\ \text{2) Advective inertia} & V\dfrac{\partial V}{\partial y} \sim \dfrac{1}{\rho_o}\dfrac{\partial P}{\partial y} \\ \text{3) Stress divergence} & \dfrac{\partial}{\partial z}\left(\nu_t \dfrac{\partial V}{\partial z}\right) \sim \dfrac{1}{\rho_o}\dfrac{\partial P}{\partial y} \end{array}\right\} \tag{2}$$

These limits represent different responses of the flow to the horizontal pressure gradient. The first is associated with unsteady momentum response, the second represents advective momentum transport and the third reflects a balance between pressure and vertical mixing.

The buoyancy equation, neglecting the alongshore component, is

$$\frac{\partial b}{\partial t} + V\frac{\partial b}{\partial y} + W\frac{\partial b}{\partial z} = -\frac{\partial \tilde{B}}{\partial z} \quad (3)$$

where $b = -\alpha g(\theta - \theta_o)$ is buoyancy, in the absence of salinity variations, and $\tilde{B}$ is the vertical buoyancy flux. Buoyancy can be scaled as:

$$b \sim \alpha g\bar{\theta} \quad (4)$$

where α is the volumetric thermal expansion coefficient, g is gravitational acceleration, and $\bar{\theta}$ is the depth averaged water temperature . The right hand side of the equation can be scaled as:

$$\tilde{B}_o/D \quad (5)$$

where surface buoyancy flux $\tilde{B}_o \sim \frac{\alpha g\tilde{H}}{\rho_o c_p}$, $\tilde{H}$ is total surface heat flux, and c_p is the heat capacity at constant pressure. Using (4) and (5) in the buoyancy equation, we obtain this scaling for the thermal energy equation:

$$\frac{\partial\bar{\theta}}{\partial t} + V\frac{\partial\bar{\theta}}{\partial y} \sim \frac{\tilde{H}}{\rho_o c_p D} \quad (6)$$

Surface heat flux will be balanced by some combination of thermal advection and unsteady temperature change. Again, the problem may be simplified if two limits are considered:

1) Unsteady temperature $\quad \frac{\partial\bar{\theta}}{\partial t} \sim \frac{\tilde{H}}{\rho_o c_p D} \quad (7)$
2) Steady temperature $\quad V\frac{\partial\bar{\theta}}{\partial y} \sim \frac{\tilde{H}}{\rho_o c_p D} \quad (8)$

For the thermal energy balance, it is assumed that although heat flux is applied to the surface, the heat is evenly distributed over the entire water column. For the steady case, the surface heat flux is compensated by a lateral advective flux, such that we would expect water temperature and surface heat flux to be in phase. For the unsteady limit, the water temperature is expected to vary as an integral of surface heat flux with respect to time. Combining the thermal energy balance with the momentum balance, a velocity scale can be determined for six regimes as shown in Table 1 (Monismith et al. 2006), where β is bottom slope, T=24 hours is the relevant forcing period, and $u_f = \left(\frac{\alpha g D\tilde{H}_o}{\rho_0 c_p}\right)^{1/3}$ is the velocity scale for convection (Fischer et al. 1979).

Table 1. Six regimes as described by Monismith et al. (2006)

	Steady temperature	Unsteady temperature
Unsteady Inertia	$V_{US} \sim (u_f^3 T/D)^{1/2}$	$V_{UU} \sim (\beta u_f^3 T^2/D^2)$
Advective Inertia	$V_{NS} \sim \beta^{-1/3} u_f$	$V_{NU} \sim (u_f^3 T/D)^{1/2}$
Stress divergence	$V_{VS} \sim u_f^{3/2}/q^{1/2}$	$V_{VU} \sim (\beta u_f^3 T/qD)$

3. Methods & Observations

Data was collected at the Kilo Nalu Observatory, located in a fringing reef environment on the south shore of Oahu, Hawaii (Figure 2) (Pawlak et al. 2009). Cabled instrumentation at the 12m isobath at Kilo Nalu includes a bottom mounted acoustic Doppler current profiler (ADCP), a thermistor chain (TChain), and a bottom conductivity-temperature sensor. The ADCP samples velocity between 2 and 11m depth at 1 Hz within 0.25m vertical bins. The bottom moored thermistor chain consists of temperature sensors spaced 1m apart from 5-11 meters depth, sampling every 3 seconds. Temperature and salinity data are collected at a 5 second interval. A surface buoy at Kilo Nalu, maintained by the Hawaii Ocean Observing System (HiOOS), also collects temperature and salinity data. A weather station located on the roof of the John A. Burns School of Medicine collects meteorological data including atmospheric pressure, relative humidity, short wave radiation, and air temperature. Wind speed and direction are acquired from the Honolulu International Airport, located 6km northwest of the Kilo Nalu Observatory. Stream flow values were obtained from the U.S. Geological Survey (USGS), and rain measurements from National Oceanic and Atmospheric Administration (NOAA) National Weather Service. From these measurements, net heat flux is calculated as the sum of short wave, latent, sensible, and net long wave radiations (Fairall et al. 1996, Fung et al. 1984), where heating is positive and cooling is negative. All data were averaged into 20 or 60 minute ensembles. The data considered in our analysis were collected over the period of January to December 2010, with significant breaks during January, July, August, and December.

A harmonic analysis of observations at Kilo Nalu shows that the alongshore currents are on the order of 10-20 cm/s and are predominately driven by the semidiurnal M2 tide (Pawlak et al. 2009). For 2010, the time-averaged alongshore velocity was about 5 cm/s to the northwest and the cross-shore was about 1 cm/s onshore. Maximum along and cross-shore velocities were on the order of 30-40 and 10-20 cm/s respectively.

In general, weather conditions are fairly constant on the south shore of Oahu. As observed, a typical day can be described as having sunny skies with scattered clouds, temperatures about 22-26 degrees Celsius, relative humidity around 60-70%, and trace amounts of rain. Trade winds coming from the northeast usually dominate the wind regime, however, when the trade winds weaken, the onshore sea breeze strengthens. On the south shore, the sea breeze brings warmer, humid air, locally referred to as “Kona wind” conditions. The weakening of the trade winds has been associated with the passage of a front, and may be accompanied by a “Kona” storm (Leopold, 1948).

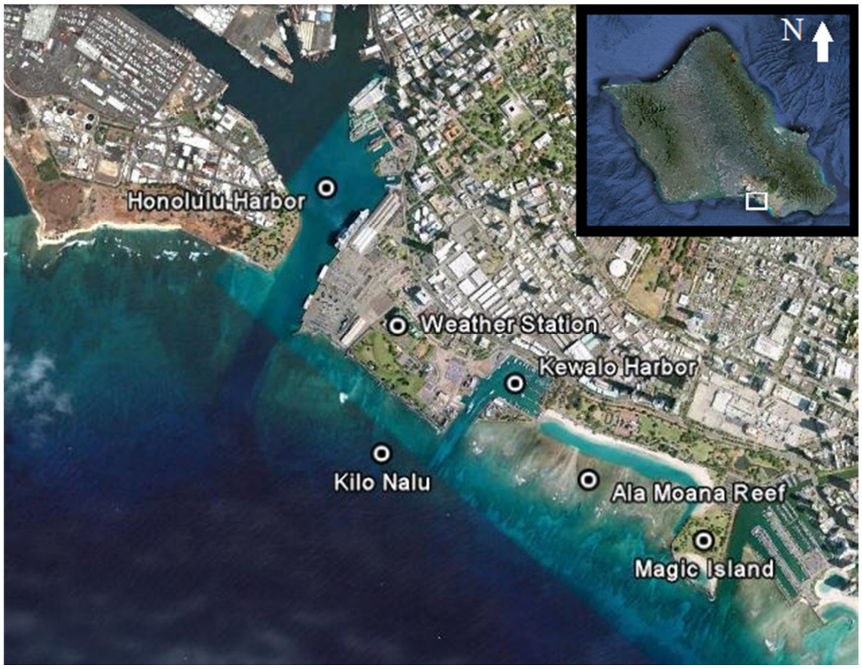

Figure 2. Map of Kilo Nalu and surrounding area, including Honolulu Harbor, Kewalo Harbor, Ala Moana Reef, Magic Island, and the location of the weather station. Inset shows island of Oahu with study site outlined in white.

4. Results and Discussion

4.1. Depth Averaged and Exchange Flow

For simplicity, we can approximate the volume inshore of the Kilo Nalu site as a two-dimensional wedge of unit width (Figure 1), where the cross-shore currents are positive onshore. The cross and along-shore directions are defined by the principal axes of the currents, which are roughly aligned with the isobaths. If the flow is purely two-dimensional so that only the cross-shore currents are considered, then the depth averaged flow must be zero. If, however, there is some net component on or offshore, it must be compensated by an alongshore divergence. For each twenty minute averaged cross-shore velocity profile in 2010, Figure 3 compares the depth averaged velocity (grey) to the average velocity magnitude (black). The velocity is always a positive value but is mirrored for the sake of comparison. The limits to consider are the pure exchange case, where the depth averaged velocity is zero, and the pure unidirectional case, where the depth averaged velocity is equal to the average magnitude. Since the depth averaged velocity is between zero and the average magnitude, the cross-shore profile is neither unidirectional nor purely an exchange flow. There is a significant net flow that is generally onshore. Potential driving mechanisms of the net flow include variations of tidal axes or other large scale, low frequency circulations. It should be recalled that the ADCP measurements do not cover about 2m of the water column at the surface. Including the surface layer, which is generally flowing offshore, may reduce the net flow. Ideally, the contribution of the exchange and the net flow would be evaluated separately by first isolating the net component from the total profile. However, because the net flow and exchange profiles are highly variable in time, a characteristic velocity profile associated with the depth averaged flow cannot be clearly defined.

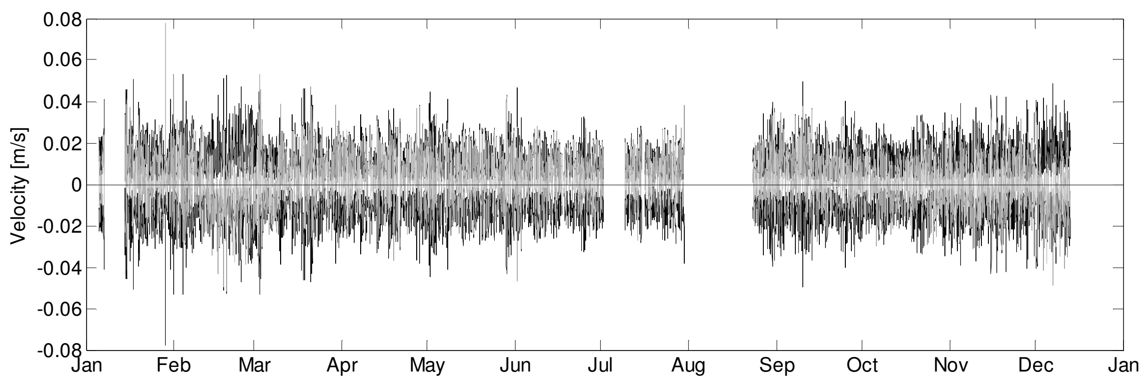

Figure 3. Comparison of depth averaged velocities (grey) to the average velocity magnitude (black) for each 20 minute averaged cross-shore current profile in 2010. Average velocity magnitude has been mirrored over the x-axis to obtain negative values.

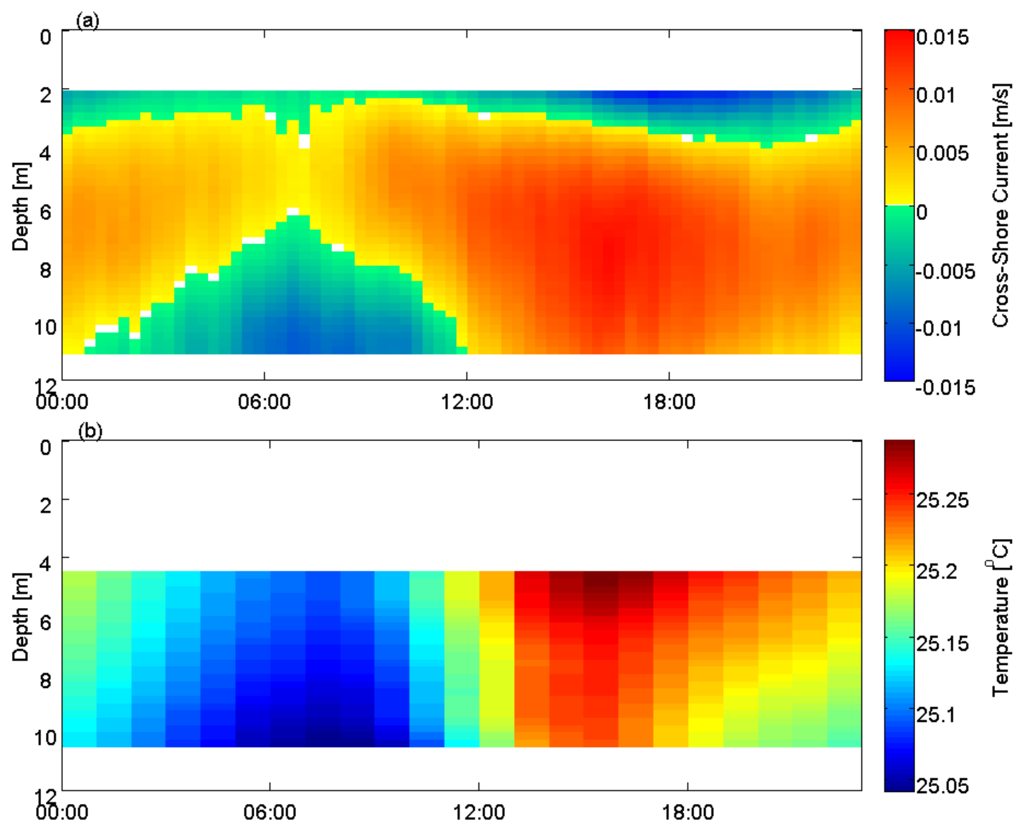

Figure 4. Diurnal average of cross-shore current profiles (a) and temperature profiles (b) from 2010.

To isolate diurnal contributions to the cross-shore currents, the velocity profiles from 2010 were averaged by hour of the day to obtain the data shown in Figure 4a. The flow near the bottom is offshore in the morning hours while the flow in the upper water column is onshore, with the exchange pattern reversing in the afternoon. The fact that the diurnal velocities averaged over an entire year are relatively strong (+/- 1.5 cm s^{-1}) in comparison with the velocities shown in Figure 3, is indicative that the diurnal exchange flow represents a significant part of the cross-shore currents.

A diurnal average of the temperature profiles shows a daily heating and cooling cycle (Figure 4b). The coldest water is at the bottom in the morning and the warmest water is near the surface in the afternoon. The diurnal pattern in exchange and the concurrent shift in the thermal structure suggest that surface heat flux may be driving the exchange. The spectra from the full data set (Figure 5) shows that both the cross- (black) and along-shore (grey) flows have a significant semidiurnal component. The M2 tidal frequency is the major contributor to the surface tide (Figure 6a) and is predominantly aligned in the alongshore direction, dominating the alongshore currents (Figure 6b). The peak in the cross-shore spectra is thus attributed to the cross-shore component of the M2 tidal ellipse. The cross-shore currents are also largely diurnal (Figure 5, black), which is often discernible in the cross-shore current data (Figure 6c).

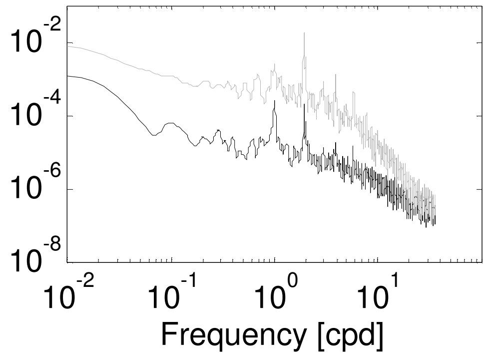

Figure 5. Spectra of the depth averaged cross-shore (black) and along-shore (grey) velocities.

Exchange volume flux is estimated for every 20 minute averaging period for the 2010 data set by subtracting the net (depth-averaged) velocity from the entire velocity profile, and then depth integrating only the onshore velocities. Short timescale fluctuations in volume flux do not contribute significantly to nearshore flushing as is evident for the case of surface waves. Volume flux will become significant to nearshore flushing at timescales over which the volume contribution is large relative to the total nearshore volume. For illustrative purposes, here, high frequency changes have been removed from the volume flux signals using a low-pass filter of 2 cycles per day. At Kilo Nalu, the exchange flux averages $0.04 m^3/s$, as seen in Figure 7, and is comparable to the net flux. The net flux is generally positive as observed previously. One way to compare the significance of the exchange flow relative to the net flow is to consider the flow rate required to flush out a two-dimensional wedge approximating the region onshore of the Kilo Nalu ADCP in a day, which is $0.03 m^3/s$. In Figure 7, this threshold is indicated by the dashed line. Both the net and exchange flux often exceed the indicated threshold, suggesting that both components are important in driving cross-shore circulation.

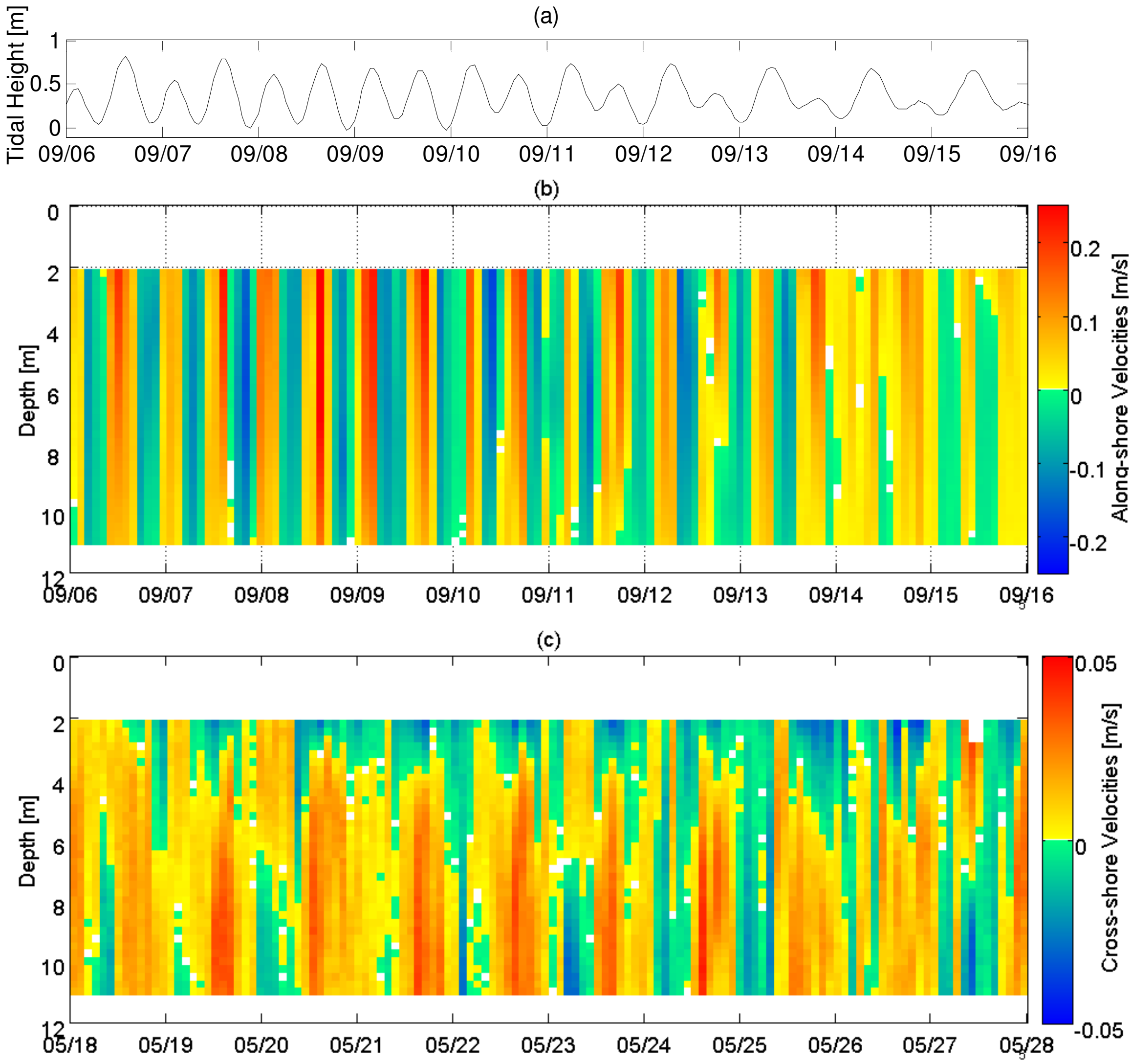

Figure 6. The semidiurnal M2 tide (a) and along-shore velocity profiles (b) from September 6-16, 2010. Cross-shore velocity profiles (c) from May 18-28, 2010, showing diurnal exchange pattern. Color indicates velocity magnitude, positive northwest (b) or onshore (c).

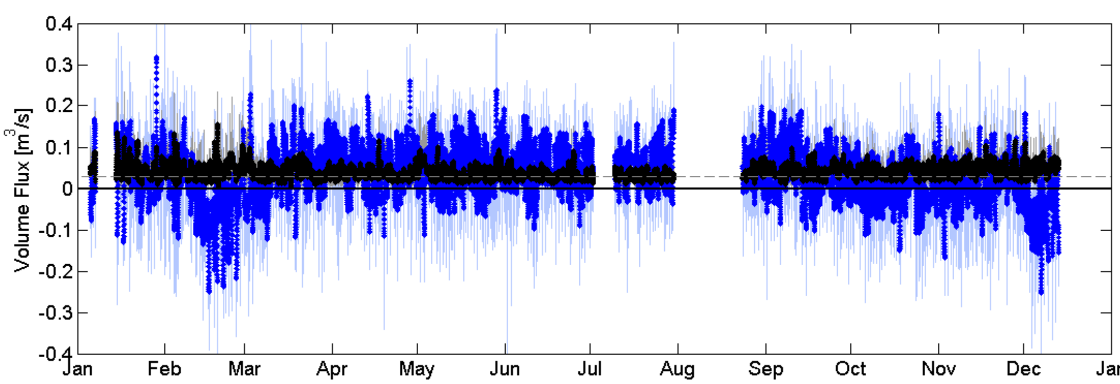

Figure 7. Exchange (black/grey) and net (blue) volume flux approximated for Kilo Nalu for 2010. Dashed line indicates flow rate required to flush Kilo Nalu area in one day.

4.2. Potential driving mechanisms of exchange

To evaluate potential driving mechanisms for the diurnal exchange flow, three different methods were used to measure the strength of the exchange over time. These measures are compared to two likely forcing mechanisms for the diurnal exchange flow, surface heat flux and wind.

Empirical Orthogonal Function

An empirical orthogonal function (EOF) analysis was carried out for the 2010 cross-shore current profiles. Figure 8 shows the vertical structures and a portion of the associated time series for EOF modes 1 and 2. These two modes account for about 57% and 31% of the current variability, respectively. The EOF spatial magnitude has been normalized such that the corresponding magnitude of the time series represents the maximum velocity magnitude in units of ms^{-1}. The sign convention is positive onshore and negative offshore. A frequency analysis of the EOF time series shows that mode 1 is mostly a diurnal signal with a weaker M2 component, whereas mode 2 is mainly M2 with a small diurnal component. The band-passed diurnal and semidiurnal components of mode 1 and 2, respectively, are highlighted in Figure 8 (b, d, red). Thus, it appears that the weak cross-shore M2 component is captured by a combination of mode 1 and 2. This would likely be characterized by a unidirectional flow with weaker flow near the bed that can be represented by a summation of modes 1 and 2. Similarly, the exchange profile observed in the diurnal average (Figure 4a) is also captured by a combination of modes. Given the relative magnitudes of the diurnal components of mode 1 and 2, however, mode 1 appears to best describe the diurnal exchange.

By averaging the surface heat flux, cross-shore and total wind magnitudes, and EOF mode 1 amplitude by hour of the day for 2010, we can evaluate the two potential forcing mechanisms by comparing their relative diurnal variation (Figure 9). Recalling that a positive EOF amplitude corresponds to a cooling exchange flow, we can see that during periods of cooling (i.e., negative heat flux) the exchange flow tends toward its cooling phase (offshore near the bed). At about 5pm, the sign of the heat flux changes from positive to negative, and concurrently, the EOF mode 1 amplitude begins to increase. The opposite occurs at about 7am when heat flux changes sign from negative to positive and mode 1 tends toward a negative amplitude; thus the response of the cross-shore exchange is well-aligned with changes in the heat flux. The depth averaged water temperature is similarly correlated with the heat flux, with a heating and cooling pattern that is shifted 180 degrees relative to the EOF mode, as seen in Figure 9.

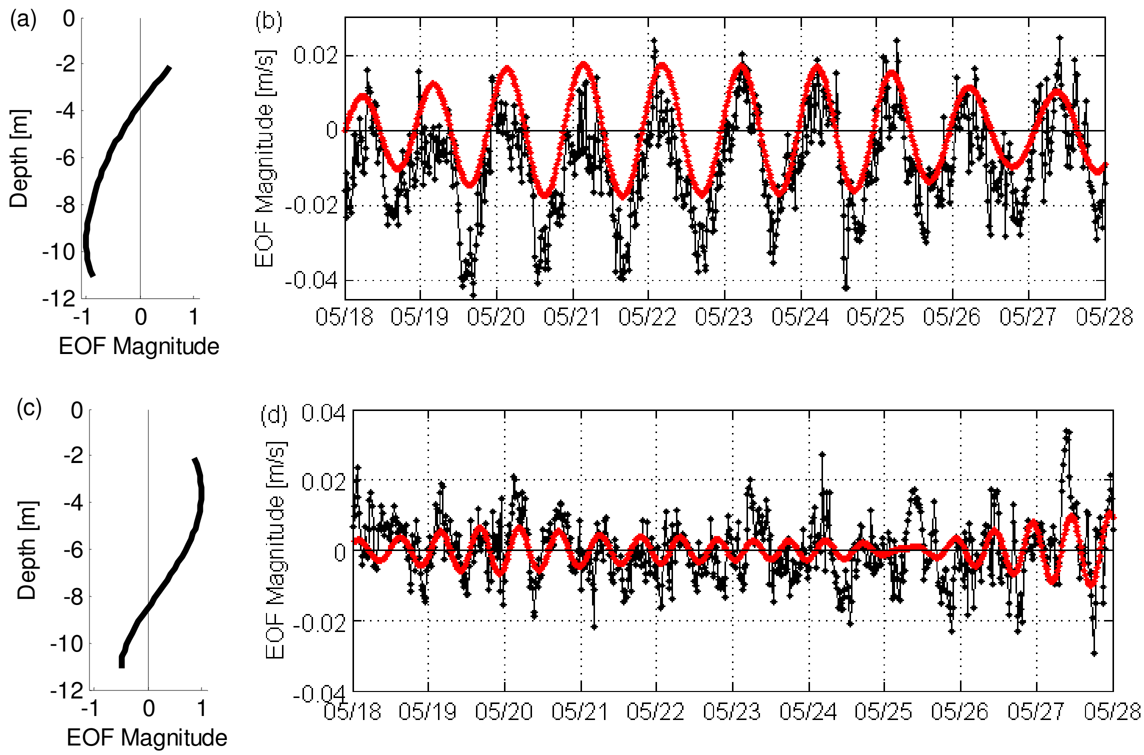

Figure 8. EOF modes 1 (a, b) and 2 (c ,d) for cross-shore velocity profiles. Associated EOF time series (b, d, black) for the period of May 18-28, 2010. Red line indicates the diurnal (b) and semidiurnal (d) bands of the signals.

There are two wind-driven mechanisms that may have an influence on the cross-shore exchange. The first is through the direct effect of surface stress forcing a surface flow in the same direction as the wind. This would be balanced by a flow in the opposite direction at depth (Fewings et al. 2008). As observed in Figure 9 (blue) the cross-shore wind magnitude does show a diurnal signal, but it is consistently in the offshore direction. Thus, wind stress cannot account for the onshore surface flow early in the day. A second possibility is that as the wind pushes water offshore in the afternoon, it sets up an exchange flow as well as a baroclinic response, such that cool water would be upwelled nearshore. In the morning, the weakening of the wind magnitude would lead to the relaxation of the baroclinic structure and the onshore flow of warm water

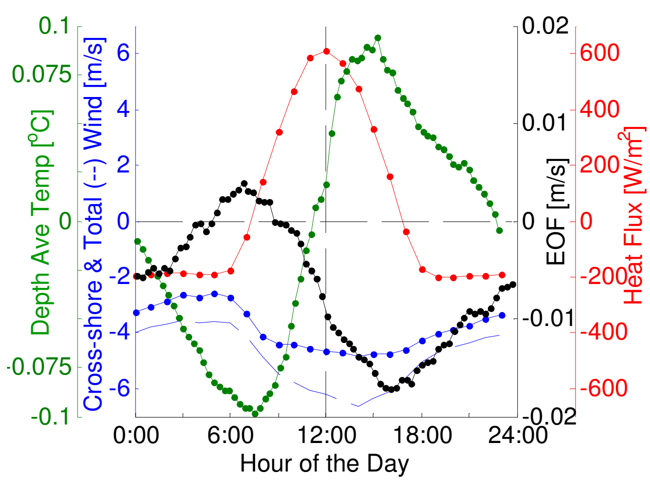

Figure 9. Diurnal composite of the depth averaged water temperature (green), wind magnitude (blue), EOF mode 1 magnitude (black), and surface heat flux (red) from 2010.

(Austin and Lentz, 2002). This baroclinic response is contradictory to observations discussed further in Chapter 2. As shown later, onshore of Kilo Nalu the warmest temperatures are observed in the afternoon and the coolest temperatures at night, the opposite of what is expected for the baroclinic response of a wind-driven exchange. So although the wind can have a direct effect on cross-shore currents via surface stress, on average, it does not appear to be the main driving factor of the Kilo Nalu cross-shore exchange. It is important to note, however, that the wind still plays a critical role in thermal exchange, driving evaporation that is the primary heat flux contribution during the cooling phase. It is also noted that the values of EOF mode 1 in Figure 9 are predominately negative, suggesting that the heating profile dominates the cross-shore currents. This is also reflected in the diurnal average of the currents in Figure 4a. It is possible that this asymmetry is due to the superposition of the diurnal exchange with a wind driven flow. The vertical profile of an offshore wind driven flow would be similar to the heating profile, thus enhancing heating profile and diminishing the cooling profile.

Although the variation in the data shown in Figure 9 indicates that the diurnal exchange is thermally driven, we must recall that EOF mode 1 does not perfectly capture the diurnal exchange. Some of the diurnal signal is lost to mode 2, and mode 1 also represents a part of the M2 tide. In addition, the diurnal component of EOF mode 1 over the period of a year (Figure 01, red) only accounts for about 50% of the variance of the unfiltered signal (Figure 10, black). While the unfiltered signal is highly variable, the diurnal component also varies significantly; however, the diurnal modulation did not show a significant correlation with the primary forcing mechanisms such as wind or heat flux. So, while EOF mode 1 seems to capture a significant amount of the diurnal exchange, it may not always be a reliable measure. This becomes more apparent when we observe the heating and cooling profiles. Heating and cooling profiles are obtained by selective averaging of the cross-shore velocities from 2010 based on hour of the day. The strongest exchange flows are observed between 3-10am for cooling and 3-10pm for heating (Figure 11). Neither of these profiles is well represented by the EOF structures in Figure 8. We also observe that the surface layer is directed offshore for both profiles, again suggesting that the wind does have an effect on the vertical structure.

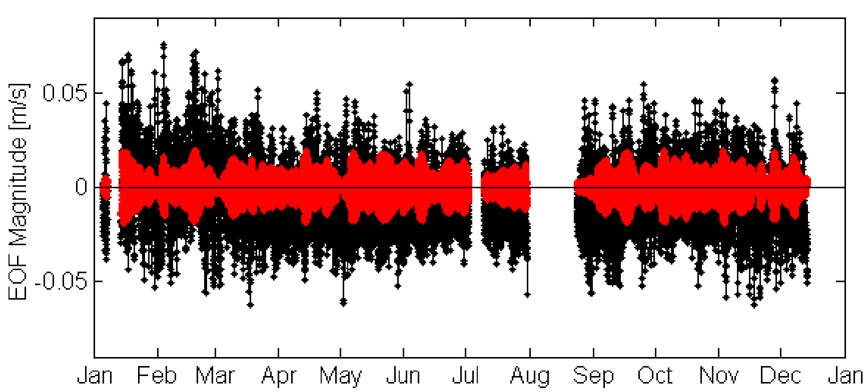

Figure 10. EOF mode 1 2010 time series (black) and the diurnal band-passed component (red).

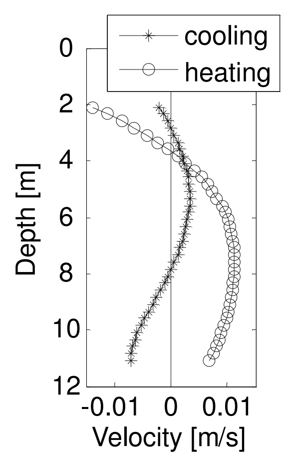

Figure 11. Average heating and cooling profiles.

Since the exchange appears to be thermally driven, we may improve our analysis by considering thermal variability along with current variability. This will help to distinguish thermal exchange from internal tidal bores, for example, which may also be captured in EOF mode 1 but can be distinguished as cold pulses of water coincident with onshore velocities (Leichter et al. 1996).

Cross-shore Shear Velocity

Monismith et al. (2006) observed cross-shore exchange over a fringing coral reef in the Gulf of Aqaba at the northern end of the Red Sea near Eilat, Israel. The cross-shore slope of 0.2 at Eilat is significantly greater than at the Kilo Nalu Observatory. While the total flow was predominately along-isobath, the cross-isobath flow was consistently dominated by a thermally-driven exchange, allowing them to use cross-shore vertical shear as a measure of the magnitude of the exchange. The diurnal average of the cross-shore shear for the Kilo Nalu observations, shown in Figure 12, indicates that in the morning, when the shear is positive, there is a cooling exchange flow. Similar to the EOF average, the shifts between cooling and heating phases coincide with the changes in heat flux (Figure 12). However, the shear is not a reliable method for measuring cross-shore exchange at Kilo Nalu because other mechanisms including wind and net flow also contribute to its variability. For the simpler bathymetry and flow at Eilat, the exchange profile for the period examined by Monismith et al. 2006 was consistent so that the cross-shore vertical shear provided a robust measure for the thermal exchange.

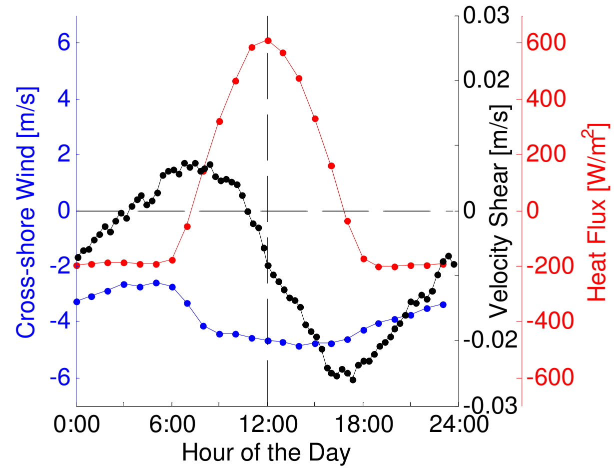

Figure 12. Diurnal composite of wind magnitude (blue), cross-shore velocity shear (black), and surface heat flux (red) from 2010.

Cross-shore Advective Heat Flux

For a thermally driven exchange, cross-shore advective heat flux can be indicative of the strength of the mechanism. We define advective heat flux as $\overline{v'T'}$, where v' and T' are the cross-shore velocity and temperature fluctuations, respectively, calculated by applying a 0.5-2.5 cycles per day (cpd) band-pass filter to the 20 minute averaged data. To observe how v' and T' vary diurnally, we plot $v'T'$ (Figures 13a, 14a, 15a). By applying a low-pass filter of 0.5 cpd to $v'T'$, we obtain a time series for $\overline{v'T'}$ (Figure 13c). Here, at Kilo Nalu, we calculate advective heat flux near the bottom at the 11m depth bin. For a thermally driven exchange, we expect to see a large positive peak in $v'T'$ during the early morning hours associated with near-bed offshore flow of cold water. The onshore near-bed flow in the afternoon is cool relative to the surface (Figure 4) but warm relative to the daily average, which should give a second smaller positive peak. The diurnal average for cross-shore advective heat flux, seen in Figure 13a, shows the expected pattern. Comparing the diurnal average cross-shore heat flux to the potential forcing mechanisms, it is apparent that peaks in the advective heat flux occur when surface heat flux changes sign (Figure 13a). This method for measuring thermal exchange has a more unambiguous physical significance relative to the EOF modes and vertical shear, but it is weighted towards the cooling period since the data represent the near-bed flow.

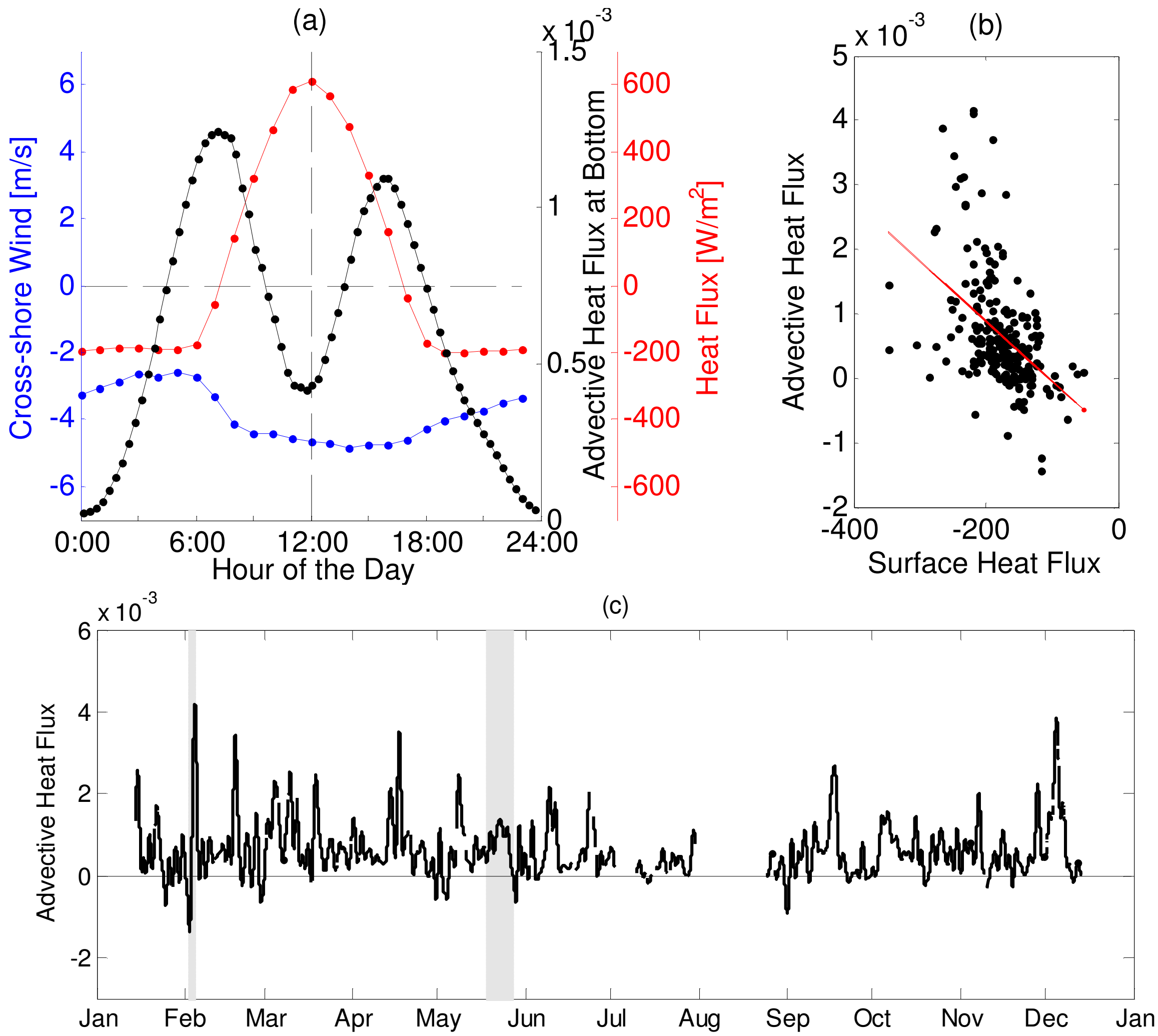

Figure 13. a) Diurnal composite of the wind magnitude (blue), advective heat flux at the bottom (black), and surface heat flux (red) from 2010. b) Correlation between advective and surface heat flux, R^2=0.23. c) Advective heat flux, $v'T'$, for 2010. Selected subsets, February 2-5 and May 18-28, are highlighted in gray.

Figure 13c shows how advective heat flux, $\overline{v'T'}$, for 2010 varies over time. It is generally positive, with occasional large positive and negative peaks. A daily measure of cooling phase magnitude is obtained by averaging $v'T'$ from midnight to noon. The corresponding daily average of surface heat flux occurs during the associated cooling phase. The cooling period is defined from the zero-crossings for surface heat flux, which typically occur around 5pm the previous day and 8am on the following morning. The daily advective heat flux defined in this manner shows a significant correlation ($p<0.01$) with surface heat flux (Figure 13b). The comparison between advective and surface heat flux includes an implicit phase lag between the forcing and response that is not well-defined. Some of the scatter in Figure 13b may be associated with variations in this lag. In addition, other advective mechanisms like internal tides and net flows will also add to the variability. Furthermore, the phase relationship between temperature and velocity may also vary in time, as discussed further below.

Although the EOF and cross-shore shear velocities are not ideal representations of the variability in exchange magnitude over time, they capture a significant portion of the exchange in their long-term diurnal averages. When averaged over a year and compared to surface heat flux averages, both show that the diurnal cross-shore exchange is thermally driven. Advective heat flux is more directly representative of thermally driven cross-shore exchange, but our measurements may be biased toward the cooling phase. Also, as discussed later, it may only represent a certain regime of thermally driven flow since it assumes that the temperature and currents are in phase and in quadrature with surface heat flux.

4.3. Temporal Variability

Temporal variations of thermally driven exchange can be expected to correlate with changes in surface heat flux and to be affected by deviations in weather patterns. For the majority of the year in Hawaii, northeast trade winds moderate temperatures and humidity (Leopold, 1948). On the south shores, wave heights vary between 0.5-2m. The wind may shift to the southwest, especially during the winter months, first bringing warmer and more humid weather, followed by larger storm waves, heavier rains, and cooler temperatures, locally termed Kona conditions (Leopold, 1948).

We will examine a selected subset of time periods where variations in forcing and the associated response in thermal exchange are illustrative of the dynamic processes that control variability. Data for May 18-28, 2010, considered previously in Figures 6 and 8, are shown in Figure 14. For this subset, where the cross-shore currents were clearly dominated by thermal exchange, we observe "normal" environmental forcing conditions with moderate trade winds, no significant rainfall, and small waves (Figure 14e, f). Surface heat flux and its components, including solar radiation, air temperature, and relative humidity, remained relatively stable (Figure 14b-d). Salinity measurements at Kilo Nalu only varied by about 0.05psu over this 10 day period (Figure 14g) and water temperatures varied diurnally with no stratification (Figure 14h). While the 20 minute averaged advective heat flux shows two positive peaks per day as expected (Figure 14a), the daily advective heat flux appears to be low during this period relative to sporadic peaks in the time series as highlighted in Figure 13c. This suggests that large positive or negative peaks of advective heat flux indicate unusual weather conditions that may not be well-correlated with the basic thermal exchange.

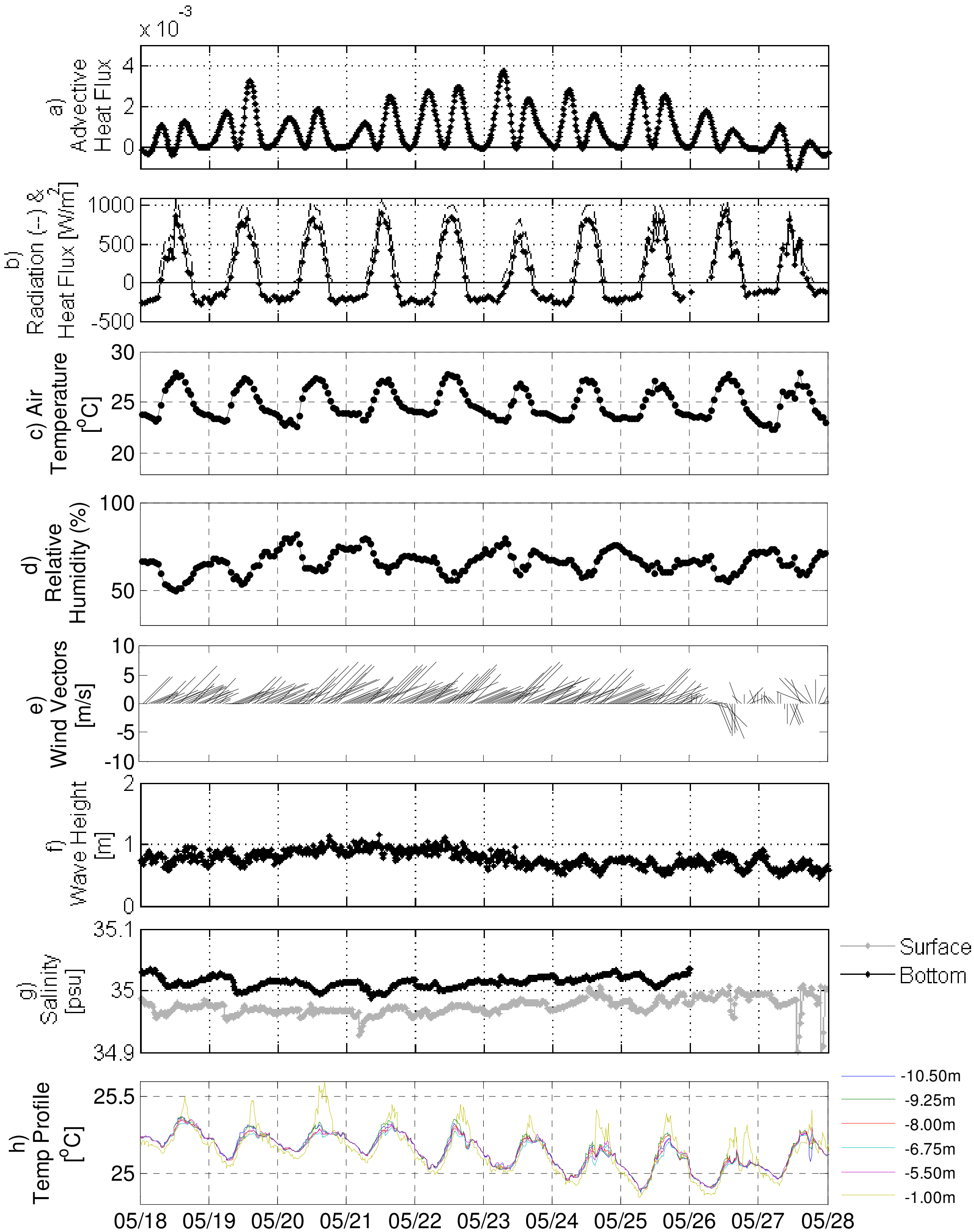

Figure 14. Environmental conditions during May 18-28, 2010.

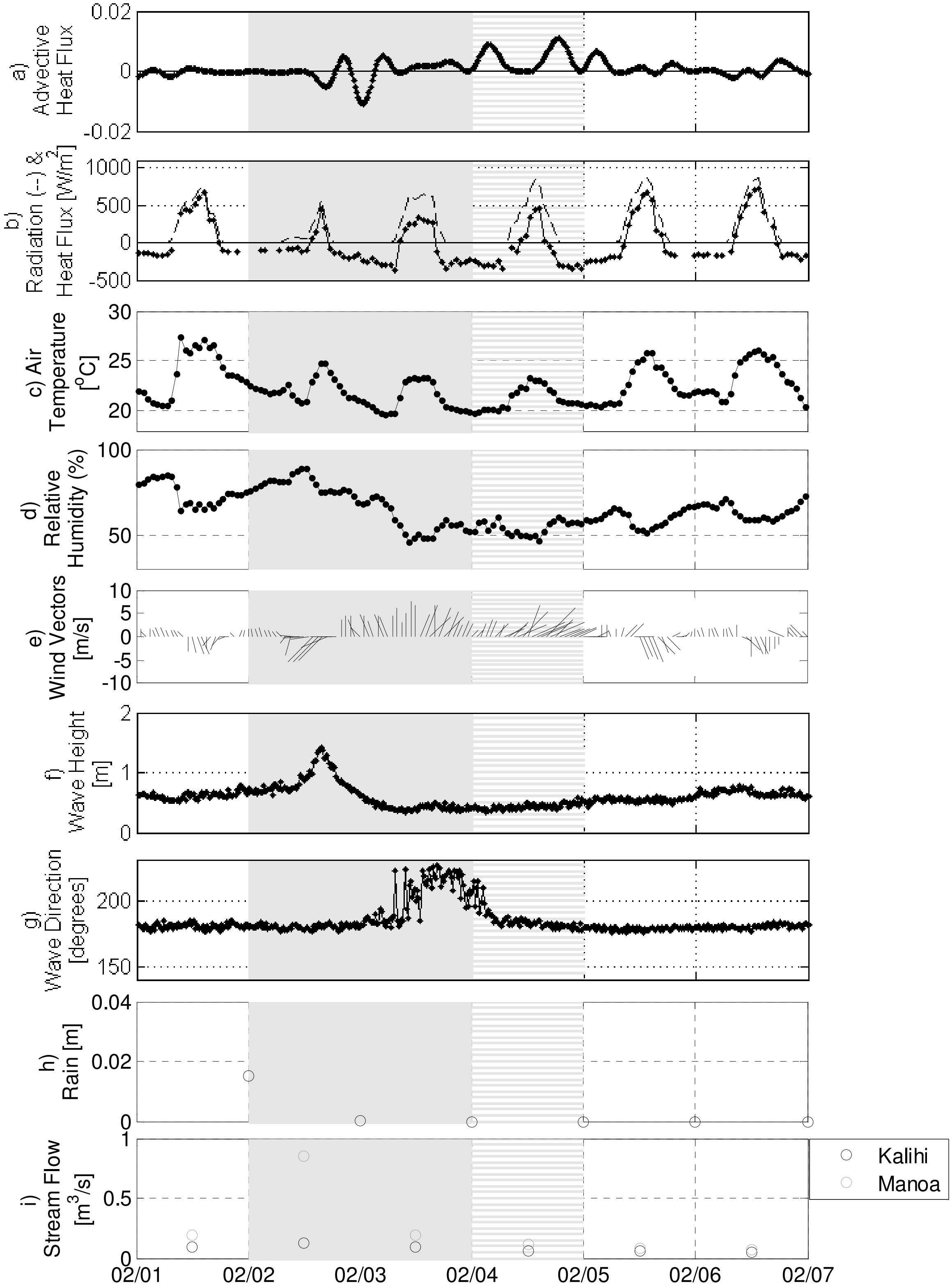

Figure 15. Environmental conditions during a Kona storm, February 2-3, 2010, followed by an unusually cold day, February 4, 2010.

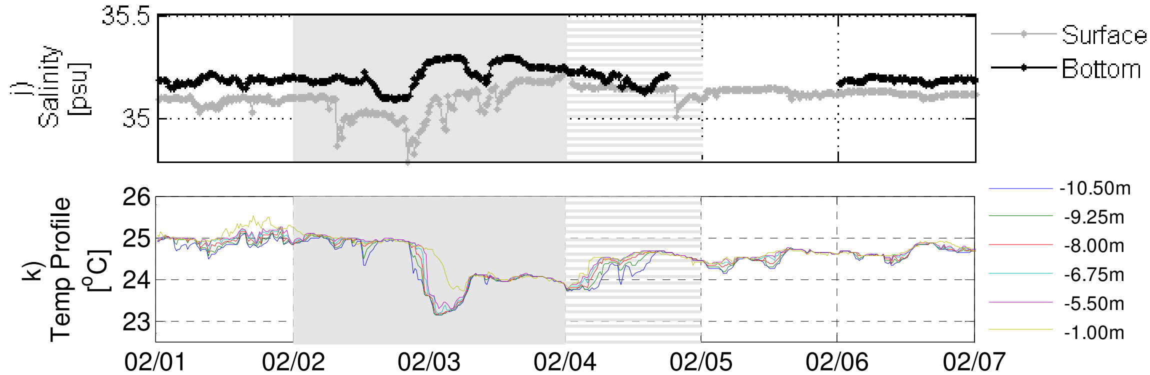

Figure 15. Continued from page 16.

For example, the large positive peak in the beginning of February, highlighted in Figure 13c, illustrates changes in the thermal exchange as a result of shifts in meteorological conditions. The negative peak in the cross-shore heat flux immediately before this positive peak, highlighted in Figure 15a, indicates that a significant event has occurred, where the currents and temperature are out of phase. For example, Kona conditions on February 2-3, 2010 (Figure 15) were marked by a drop in surface heat flux due to decreased solar radiation. Increased cooling was accompanied by high relative humidity, ~90%, followed by a large drop to ~40%. The wind and waves came out of the southwest (Kona conditions), accompanied by increased rain, stream flow, and wave heights. The passage of the cold front set up ideal conditions for strong cooling the following day. On February 4, 2010, there was on overall drop in surface heat flux due to cooler air temperatures and low relative humidity, while all other conditions appeared normal. This led to strong advection, as shown by the large positive peak in advective heat flux (Figure 15). Other environmental changes, such as large rain events or internal tides, may also cause the thermal exchange mechanism to be masked or altered.

4.4. Dynamics of thermally driven exchange

Recalling the scaling arguments for V summarized in Table 1, we can attempt to determine which regime best describes the cross-shore exchange at Kilo Nalu by examining variations in the exchange relative to the forcing parameters. Here, the strength of the exchange, V, is represented by the daily average of cross-shore heat flux during cooling. For the Kilo Nalu 12m node observations, the values of T, D, and β are constant, thus the only variables that allow us to discriminate between the unsteady inertia, advective inertia, and stress divergence are u_f and u_*. The regimes presented in Table 1, therefore, can only be differentiated into two groups, u_f and ${u_f}^3/u_*$. By examining the variations of V relative to these two parameters (Figure 16) we see that there is significant scatter in both groups, although a relationship is more clearly notable versus u_f alone, which indicates an inertial balance (Table 1). Since u_f is proportional to $\widetilde{H}^{1/3}$, the data in Figure 16a are identical to that in Figure 13b, but with the horizontal axis scaled accordingly.

By reexamining Figure 9, we see that the water temperature is in quadrature with the surface heat flux. This suggests that the temperature balance is in the unsteady regime, where the temperature in determined from the time integrated surface heat flux (i.e., Eq.

7). It is important to note that the cross-shore thermal gradient is unresolved for this time period, however, so the regime cannot be established conclusively. However, if the temperature balance were in the steady regime, we would expect the water temperature to be in phase with heat flux (i.e., Eq. 8).

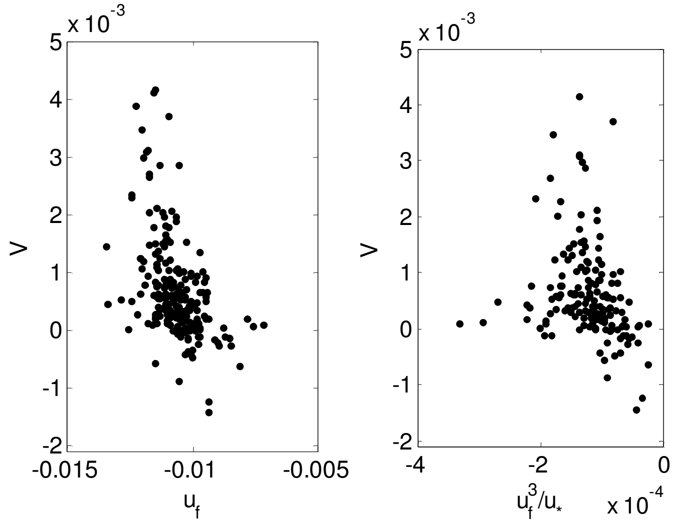

Figure 16. Relation of advective heat flux, *V,* to u_f and $u_f{}^3/u_*$.

For comparison, Monismith et al. 2006 qualified the flow regime for Eilat, Israel as steady temperature, advective inertia. Phillips (1966) derived the same scaling to describe larger scale convective circulation in the Red Sea. The temperature balance appears to be different at Kilo Nalu, while the momentum balance does not show a clear regime. This is likely due to the fact that many other factors are contributing to the cross-shore flow, such as shoaling internal waves (Pawlak et al. 2009), thus affecting the mechanism of cross-shore exchange. It is also likely that the flow is best described by different regimes throughout a single day. With a longer time series, it may be possible then to identify the flow regimes at Kilo Nalu by introducing other discerning factors such as time of day, periods with internal bores, or wind strength.

There are two important points to acknowledge about our calculations. First, we assumed that if there is a thermally driven exchange, velocity would be in phase with water temperature, which was observed on average. As was discussed in Section 2, however, for the steady temperature regime we would expect water temperature to be in phase with surface heat flux, introducing a possible phase shift between the temperature and velocity response. In this case, it is also likely that different momentum regimes would also lead to different phasing for water velocity. Thus, our calculation of advective heat flux, $\overline{v'T'}$, may not always be a reliable method for identifying thermally driven exchange. The second point is that because u_f is directly proportional to $\widetilde{H}$, the relationships shown in Figure 16 depend heavily upon the correlation between advective heat flux and surface heat flux, which was shown in Figure 13b. While clearly correlated, the scatter observed in Figure 13b carries over to the regime analysis, making it difficult to come to a significant conclusion about flow regimes.

5. Conclusions

Our observations show that cross-shore flow at Kilo Nalu includes a significant baroclinic exchange driven by thermal forcing. The baroclinic flow is comparable in magnitude to the depth-averaged component, although some uncertainty is introduced by lack of data near the surface. For the thermal exchange, currents are offshore at the bottom during cooling and offshore at the surface during heating phases. Based on the diurnal averages (Figures 9, 12, 13a), diurnal patterns in the exchange flow match that for net surface heat flux. Neither wind nor waves can account for the cross-shore exchange because they do not change direction diurnally. However, wind is an important factor in determining the amount of cooling that will occur on a given day via its effect of surface heat flux through evaporative cooling. Waves may be of secondary importance by determining the flushing time closer to shore where wave driven circulation likely dominates. A shorter flushing time would lead to greater heating of the nearshore waters and could increase the strength of the exchange observed at the 12m isobath. A vertical exchange structure consistently describes over 50% of the observed variation of the cross-shore currents based on the EOF analysis, is significant when compared to the net flow, and shows up clearly in diurnal averages over a year-long period. The near-bottom advective heat flux provides a generally reliable method for quantifying the thermally driven exchange. We see that it is well correlated with surface heat flux over time, but there are no notable seasonal changes.

The thermally driven exchange at Kilo Nalu appears to be in the unsteady temperature regime based on the phase relationship between temperature and surface heat flux. The flow can be differentiated as being inertially dominated, but the unsteady and advective regimes are not distinguishable. This is likely due to complexity in forcing dynamics, where spatial variability, internal tides, wind and waves may play a role. It is also likely that the flow progresses through different dynamic regimes throughout the day, making it difficult to assign a single regime to describe Kilo Nalu. There are also several environmental factors that may affect or mask the thermal exchange including storms, rain events, and internal tides. Furthermore, although it is apparent that thermally driven exchange is an important mechanism at Kilo Nalu, the two-dimensional approximation appears to be an over simplification of the nearshore area. The complexity of the shoreline (Figure 2) suggests that spatial variability is an important factor in understanding this mechanism.

To further study this problem, a three-dimensional approach should be taken, to observe how this mechanism varies in time and space. In order to have measurements for each term in the thermal energy and momentum equations, a horizontal gradient of temperature and current needs to be established. Surface measurements are also important for capturing the heating phase. Overall, the robustness of the signal has allowed us to identify thermally driven exchange as an important mechanism in the cross-shore dynamics at Kilo Nalu.

Chapter 2. Spatial Variability Affecting Cross-shore Thermal Exchange at Kilo Nalu

1. Introduction

Thermally driven exchange dominates the cross-shore circulation at Kilo Nalu Observatory, however, our studies have shown that the problem cannot be fully described by a two-dimensional analysis. A 2D scenario implies that physical features and dynamics are uniform in the long-shore direction. In the 2D case, a nearshore area with a sloping bottom may be represented as a wedge. The mechanism of thermally driven exchange, as studied by Monismith et al. (2006), is established by changes in temperature resulting from the cross-shore change in depth. Other research has shown, however, that a similar mechanism can be observed between a shallow area connected to a deeper region, such as a lagoon connected to the ocean (Boden, 1952). Near Kilo Nalu there are a few semi-enclosed regions, including Honolulu Harbor, Kewalo Harbor, and Ala Moana Lagoon, where water temperature fluctuations may be greater than offshore. This complex shoreline suggests that the horizontal thermal gradient driving cross-shore exchange may be modified by shallow regions located alongshore of the Kilo Nalu site. Thus, alongshore variability could play a significant role in the cross-shore dynamics observed at Kilo Nalu.

For some insight on the role and significance of spatial variability, a short experiment was designed to measure nearshore water properties from Honolulu Harbor to Ala Moana lagoon. More focus was placed on the Ala Moana area since the reef, which connects the lagoon to the open ocean, is nearest to Kilo Nalu. Although the current patterns in the reef-lagoon system are unknown, a simple description would be that wave-driven flow forces water over the reef into the lagoon. The water must then exit the lagoon through the channels on the outer edge of the reef. For our study, measurements of temperature and salinity can indicate whether or not this area is a source of buoyancy, potentially driving cross-shore exchange at Kilo Nalu.

2. Experimental Design

The aim of this experiment was to collect temperature and salinity measurements over a large region, but focused over a short period of time. We specifically wanted to capture the peak of a cooling phase (~5-6am) and the transition to heating (~10-11am). An array of six temperature sensors was placed on Ala Moana reef approximately 1m below mean sea level with an additional sensor floating one meter below the surface at Kewalo Harbor to measure water temperatures from April 27 to May 6, 2011 (Figure 1, colored points). Of these seven sensors, instrument number 7 was recovered shortly after deployment on April 27th and instruments 1 and 5 were recovered mid-day on April 29th. During this 10 day period, an acoustic Doppler current profiler (ADCP), thermistor chain (TChain), and surface buoy were deployed at the Kilo Nalu 12m site providing temperature and current profiles and surface salinity measurements.

During the morning of April 29, 2011, from about 5-11am, three other instruments were used to expand the dataset. A REMUS-100 (Hydroid Inc.) autonomous underwater vehicle (AUV), traveled at 4.5 knots in triangle profiles near the 8m isobath traveling from the eastern end of Ala Moana reef to Honolulu Harbor, a total of about 4km. On the return trip, REMUS stayed 3 m above the bottom and swam three offshore legs at Kilo Nalu (Figure 1, white tracks). REMUS was able to make three round trips during this morning period. On the third return leg, REMUS travelled at a constant depth of 2m rather than following the bottom in order to resolve water property changes associated with surface heating. While REMUS was equipped with many sensors, only the temperature and salinity data were used for this analysis.

That same morning, additional temperature and salinity measurements were concentrated around Ala Moana reef. A Seabird 16 was attached to an ocean kayak in order to take surface measurements in the lagoon. Taking about 45 minutes per round trip, a handheld GPS was used to track the location of the measurements (Figure 1, black tracks). A Seabird 37 was used to take profiles at 10 predetermined locations around the reef (Figure 1, numbers KP1-10). A total of 57 profiles were taken. Table 1 summarizes the instruments used and sampling information.

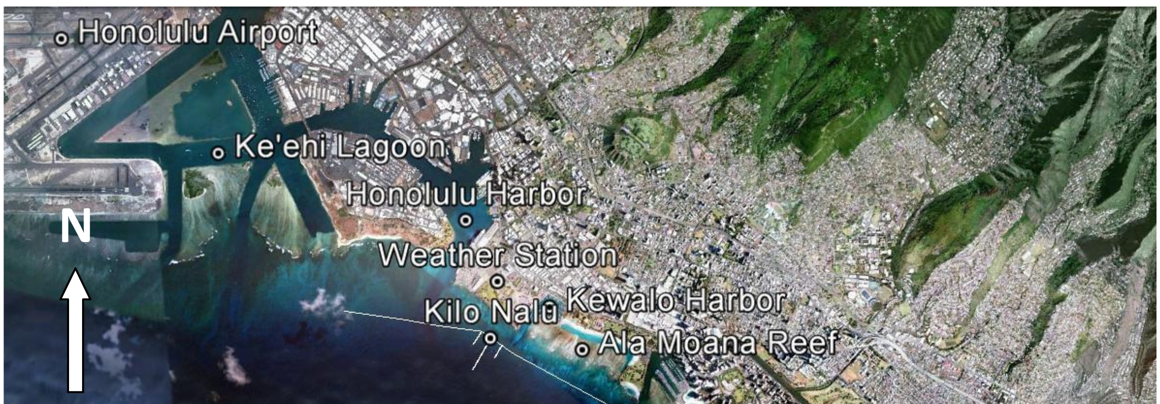

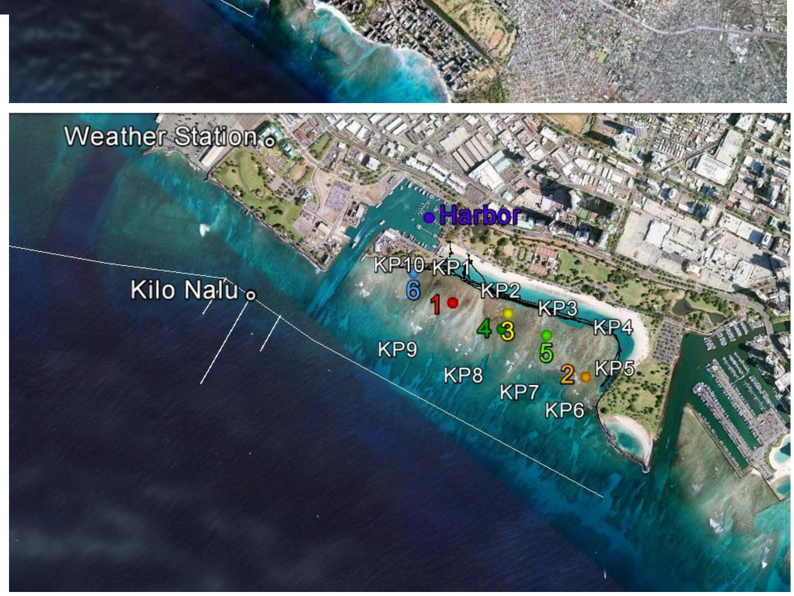

Figure 1. Map of south shore Oahu. Locations of Honolulu Airport, Ke'ehi Lagoon, Honolulu Harbor, Kewalo Harbor, and Kilo Nalu Observatory and weather station are labeled. White line shows path of AUV mission. Inset shows a close up of the Ala Moana reef and lagoon areas. Black line indicates the track of surface measurements, points KP1-10 are locations of the profiles, and temperature sensor locations are marked by colored numbers and points.

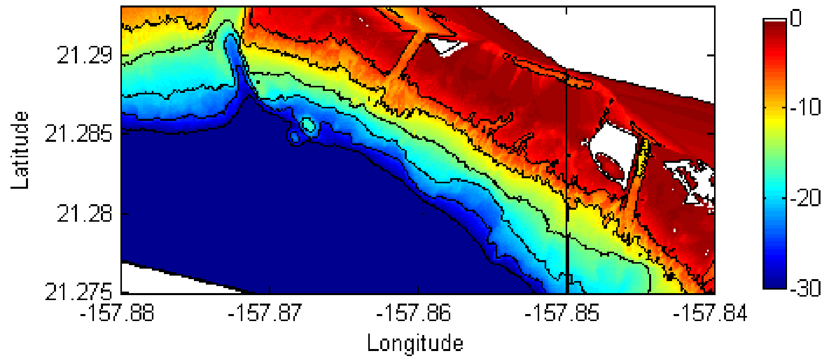

Figure 2. Bathymetry of south shore Oahu.

Table 1. List of instrumentation used and data collected.

Instrument Type	**Deployment Platform**	**Data Collected** (T=temperature, S=salinity, P=pressure)	**Sampling Period**	**Sampling Rate**
Seabird 49 CTD	REMUS AUV	T, S, P	April 29, 2011	1 second
Seabird 16 CT	Kayak	T, S	April 29, 2011	10 seconds
Seabird 37 CTD	Kayak	T, S, P	April 29, 2011	5 seconds
Seabird 39 Thermistor (quantity: 7)	Bottom mounted (1-6), floating (7)	T	April 27-May 6, 2011	30 seconds
ADCP	Bottom mounted	Current velocity	April 27-May 6, 2011	1 second
TChain	Bottom moored	T	April 27-May 6, 2011	3 seconds
Surface Buoy	Bottom moored	T, S	April 27-May 6, 2011	20 minutes

3. Observations

3.1. Background Conditions

Measurements taken at the Kilo Nalu 12m site and at the Kilo Nalu and Honolulu International airport weather stations provide background conditions for the 10 day period from April 27 to May 6, 2011. Unfortunately, during this period, a clear thermally driven cross-shore exchange structure (i.e., Figure 5a, Chpt. 1) is not evident in the cross-shore current profiles (Figure 3a). Water temperatures show a fairly typical diurnal variation and stratification is weak except for two large cold pulses on the 30th and 2nd and one smaller pulse on the 29th (Figure 3b). Winds, shown in Figure 3c, were mostly from the northeast during this period. Despite data gaps in the record, time series (Figure

3e, f) show relatively lower values for surface heat flux, solar radiation and air temperature plots on April 29th and May 1-2nd. On the 29th, relative humidity (Figure 3g) was high during the day, followed by a large drop on the 30th. Waves were fairly small over the study period, with peak swell direction from the south and southwest (Figure 3h). Surface salinity was relatively constant until May 2nd where we observe a freshening, likely due to the increased stream flow and rain (Figure 3 i-k).

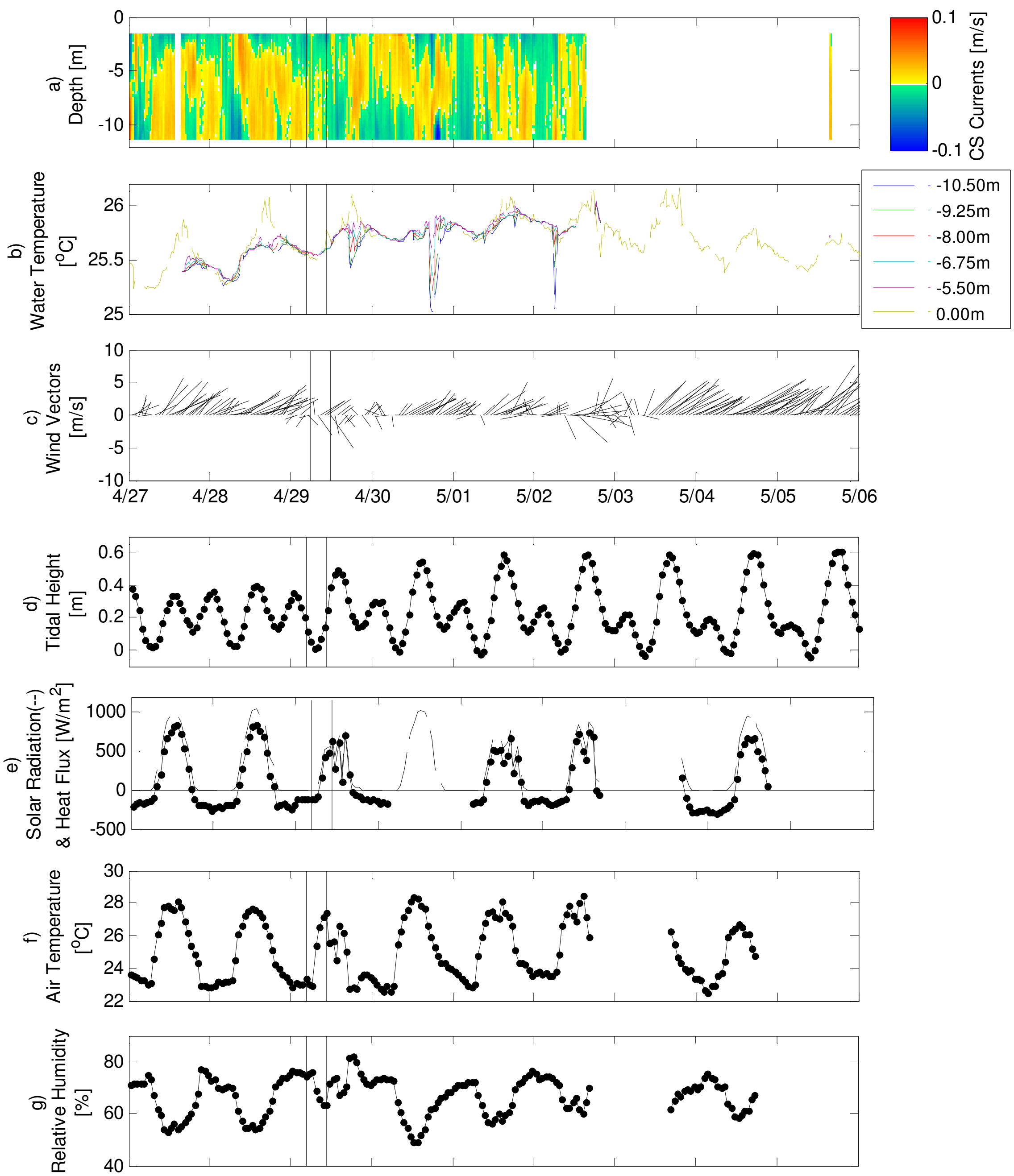

Figure 3. Environmental conditions April 27 – May 6, 2011 including cross-shore currents, water temperatures, wind vectors, tidal height, surface heat flux, solar radiation, air temperature, relative humidity, significant wave height, surface salinity, rain and stream flow.

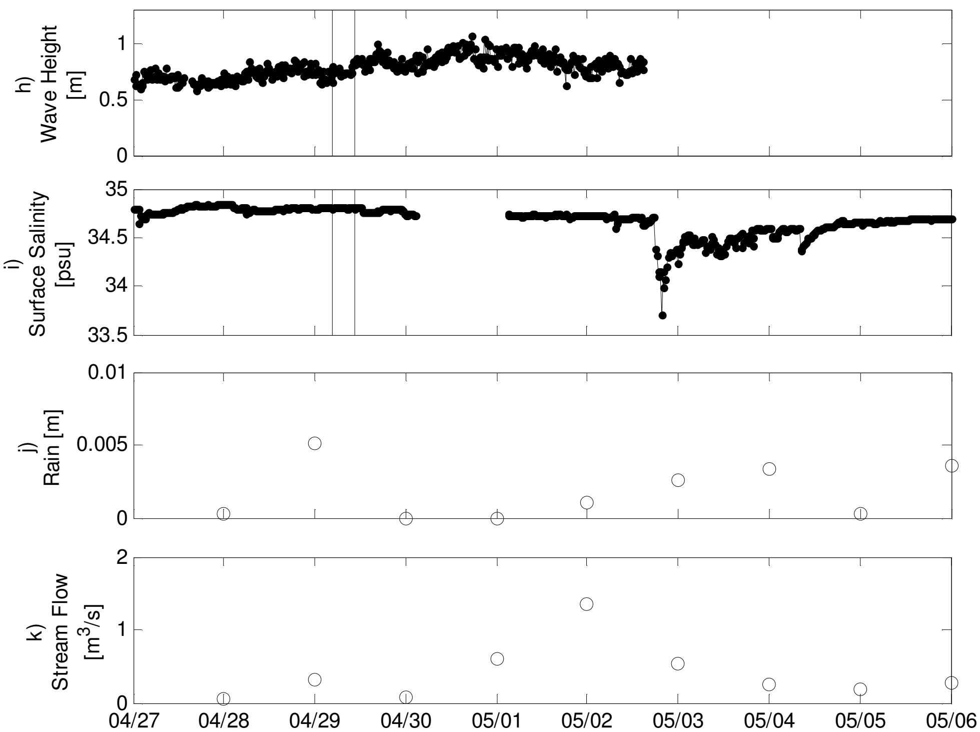

Figure 3. Continued from page 23.

3.2. Ala Moana Reef

In Figure 4, the temperatures measured over Ala Moana reef and in Kewalo Harbor are compared to the temperatures offshore at Kilo Nalu. It is clear that the temperatures on the reef (24-29^{o}C) have a greater range than those at Kilo Nalu (25-26^{o}C). Kewalo Harbor is consistently warmer than Kilo Nalu surface and bottom temperatures. Since the Kewalo measurement was at the surface and there was no bottom sensor, it is difficult to say whether or not the cold water generated at night was colder than observations at Kilo Nalu. Sensors numbered 1, 2, and 5 show that the east and west areas of the reef are consistently colder at night while the middle region (sensors 3 and 4) only sometimes drops below Kilo Nalu temperatures. This spatial variability in temperature is indicative of a more complex circulation pattern than the simple case described earlier. Overall, the temperature comparison between near and offshore waters shows that the shallow nearshore waters both heat and cool to a greater degree than offshore. This supports the observations of thermally driven exchange at Kilo Nalu and further suggests that the reef-lagoon system at Ala Moana plays an important role in establishing the necessary cross-shore thermal gradient that drives this mechanism.

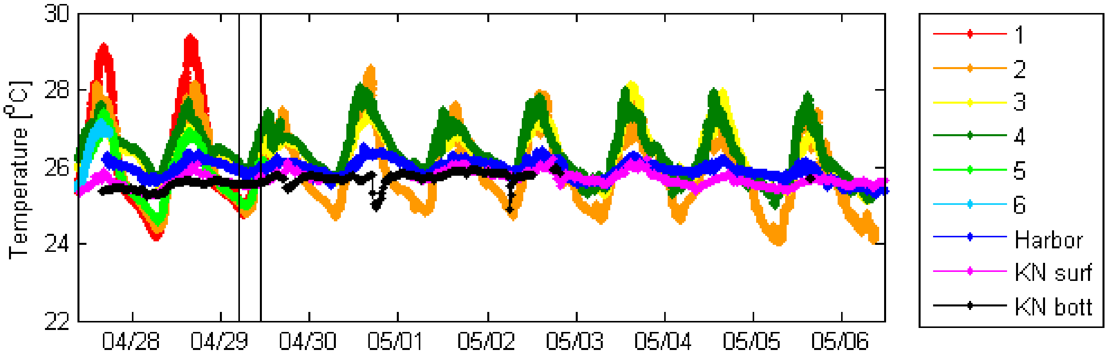

Figure 4. Water temperature on Ala Moana reef (1-6), Honolulu Harbor, and at the surface and bottom of Kilo Nalu. Colors and numbers correspond to locations on map in Figure 1. Vertical lines indicate the period of the experiment on April 29, 2011.

3.3. Offshore Ala Moana

Although the AUV ranged from Ala Moana to Honolulu Harbor, our analysis will focus on the area directly offshore of the Ala Moana reef. Temperature and salinity measurements were averaged horizontally from 0-1700m (Figure 5) to obtain profiles (Figure 6a, b) and vertically averaged over 2-8m depth to obtain transects (Figure 6c, d) for each REMUS leg. The data coverage for each leg can be seen in Figure 7. When comparing the transects, it should be noted that the last transect only represents an average over the top 2.5m since the last leg only took surface measurements.

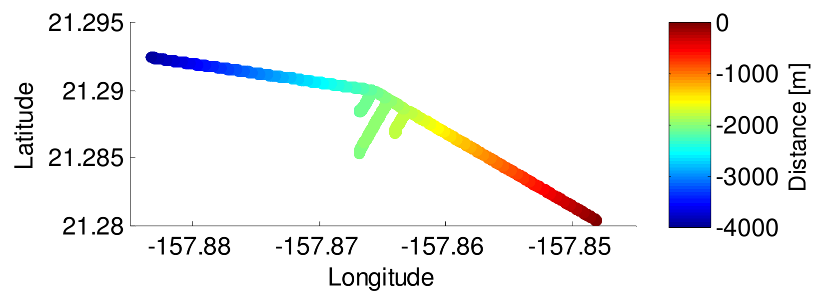

Figure 5. REMUS track showing measured distance from start location.

The temperature profiles are relatively constant over depth, but we observe the water first cooling then warming, corresponding to heat flux switching from a cooling to heating phase at about 7:00am. However, the temperature range is fairly small, about 0.1^{o}C, compared to measurements on the reef, which increase about 2^{o}C over the same period (Figure 4).

The salinity profile is fairly constant both over depth and time, except for a fresh point near the surface at about 11am. This can be attributed to the Ala Wai Canal, which is located to the east of Ala Moana. The depth averaged alongshore currents (Figure 8), which are westward and increasing in strength during this study period, bring fresh water from the Ala Wai plume toward the Ala Moana area.

The temperature transects also show the cooling and heating cycle, but in addition there is a notable spatial pattern. A region of cooler water is evident offshore of the central region of the reef. The pattern persists over a number of transects. Notably, this is in contrast to the relatively warmer temperatures observed on the middle of the reef (Figure 4). The salinity transect also shows that a shift occurs in the mid reef region. The waters to the east are slightly fresher, especially at 10:50am. Again, this is likely associated with the Ala Wai plume.

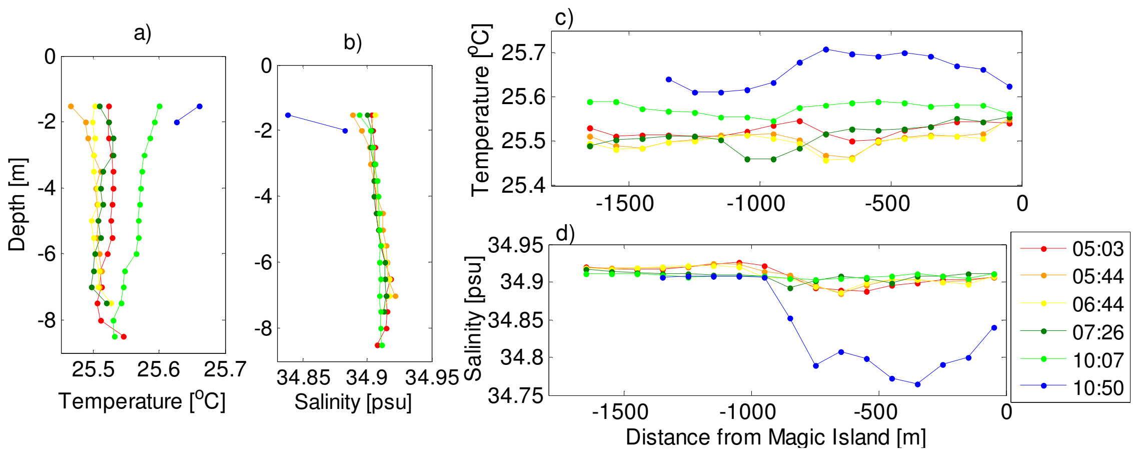

Figure 6. Temperature and salinity profiles (a, b) and transects (c, d) taken by REMUS offshore of Ala Moana reef. Measurements were made from 1-9 meters from 5-11am on April 29, 2011.

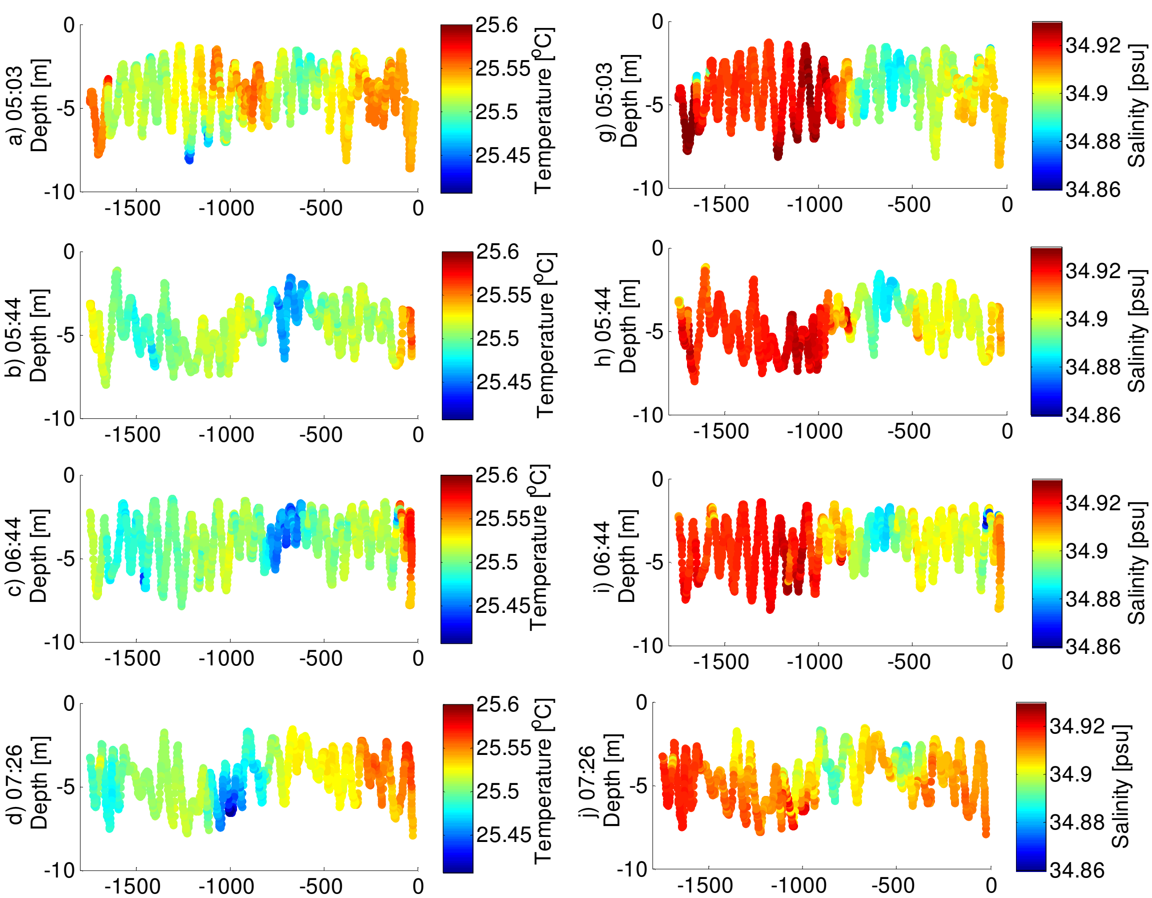

Figure 7. REMUS measurements of temperature (a-f) and salinity (g-l) in front of Ala Moana.

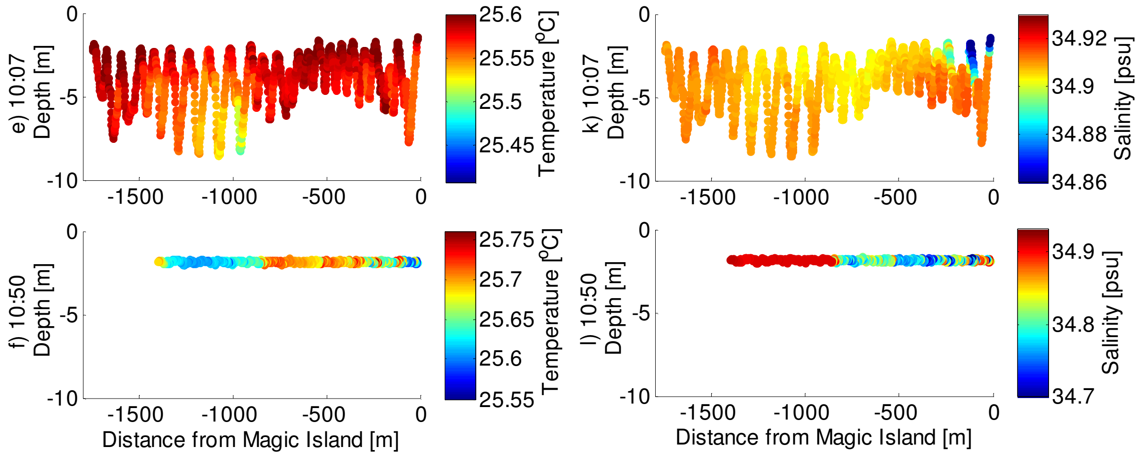

Figure 7. Continued from page 26.

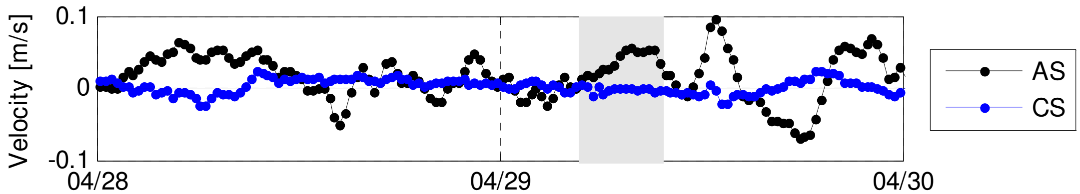

Figure 8. Depth averaged along-shore (black) and cross-shore (blue) currents during April 28-29, 2011. Focused study area highlighted in gray.

3.4. Ala Moana Lagoon

Surface measurements were obtained in the Ala Moana lagoon near the reef using a kayak, as shown by the tracks in Figure 1. The colored points in Figure 9 show temperature and salinity as a function of distance from the northeastern point of the lagoon. The larger points represent the main part of the lagoon and were averaged over each track to obtain a time series as shown in Figure 10. The smaller points in Figure 9 are attributed to the east or west channels. The lagoon is compared to the offshore measurements taken by REMUS (Figure 9, black lines) and at Kilo Nalu (Figure 9, black & magenta), where the relative distance is shown by the x-axis. In the temperature plot we see that the lagoon was generally warmer than offshore. In the early morning, the channels were about 0.5^{o}C colder than the lagoon. Overall, there seems to be a significant shift mid-lagoon, the east side being slightly colder. The range in temperature over this time period is about 1 degree, less than over the reef-top (Figure 4) but greater than offshore. From Figure 10a, we see that over the period observed, the lagoon cooled and heated, similar to the REMUS observations (Figure 6).

During the last leg (Figure 9a), a few jumps in temperature were observed mid-reef. By this time, the thermal forcing has transitioned to the heating phase, and we can expect that the highest temperatures will be over the reef. These jumps in temperature (Figure 9a) are likely associated with regions of warmer water flowing on the surface from the reef-top into the lagoon. It is notable that similar cold pulses are not evident in the lagoon during the cooling phase observations, although lower temperatures are observed on the reef flat. This is likely because cool water flowing off the reef would rapidly sink within the warmer lagoon.

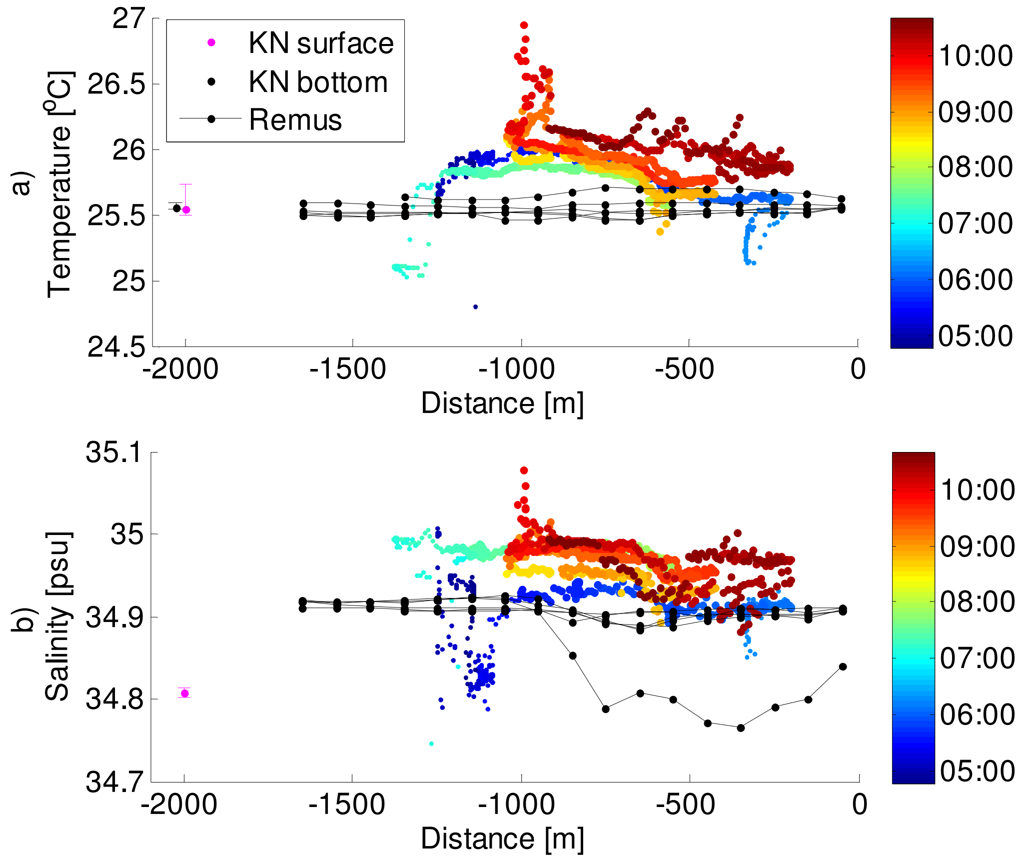

Figure 9. Colored points show surface temperature (a) and salinity (b) measurements as a function of location and time in Ala Moana lagoon. Black line indicates measurements made by AUV directly offshore (same as Figure 6c, d). Black and magenta points at 2000m are measurements made at Kilo Nalu during the same time period.

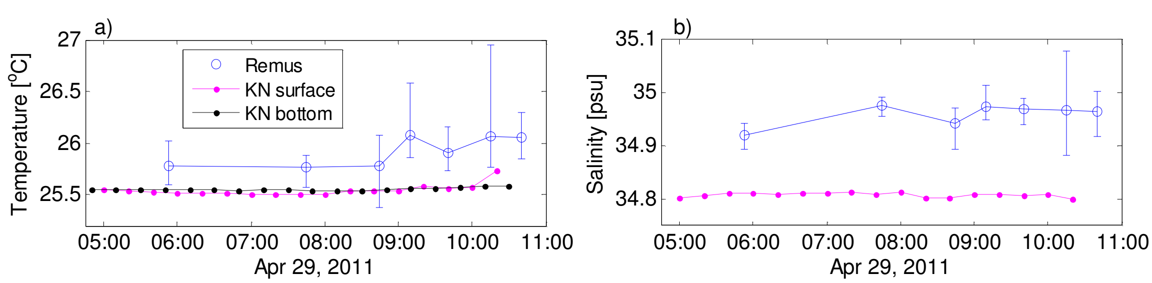

Figure 10. Surface temperature and salinity in Ala Moana lagoon averaged based on transect time as seen in Figure 9.

The salinity plots show similar trends. The lagoon was generally more saline than offshore (Figures 9, 10). As seen in Figure 9b, the eastern part of the lagoon is slightly fresher, as is reflected in the REMUS observations just offshore. The decrease in salinity is consistent with the influence of the Ala Wai Canal located just to the east. Surface salinity generally increased in the lagoon over the day (Figure 10b). The Kilo Nalu surface measurements were approximately 0.15psu less than the Ala Moana area.

3.5. Ala Moana Profiles

Four sets of temperature and salinity profiles were taken at six different points in Ala Moana lagoon from 5-11am. Figure 11 shows contours of temperature and density based on these profiles, where the x-axis is distance from the eastern channel and black vertical lines indicate locations of actual measurements. In the temperature plot, we observe a gradient from the east to the west. Throughout the morning the coldest temperatures are seen on the eastern end of the lagoon, while the temperatures in the western end increase more rapidly such that there is almost a 1^{o}C difference across the lagoon by late morning. There is a similar tilt to the isopycnals. Throughout the morning, less dense water is generated at the surface, primarily due to heating but also in part to a decrease in salinity.

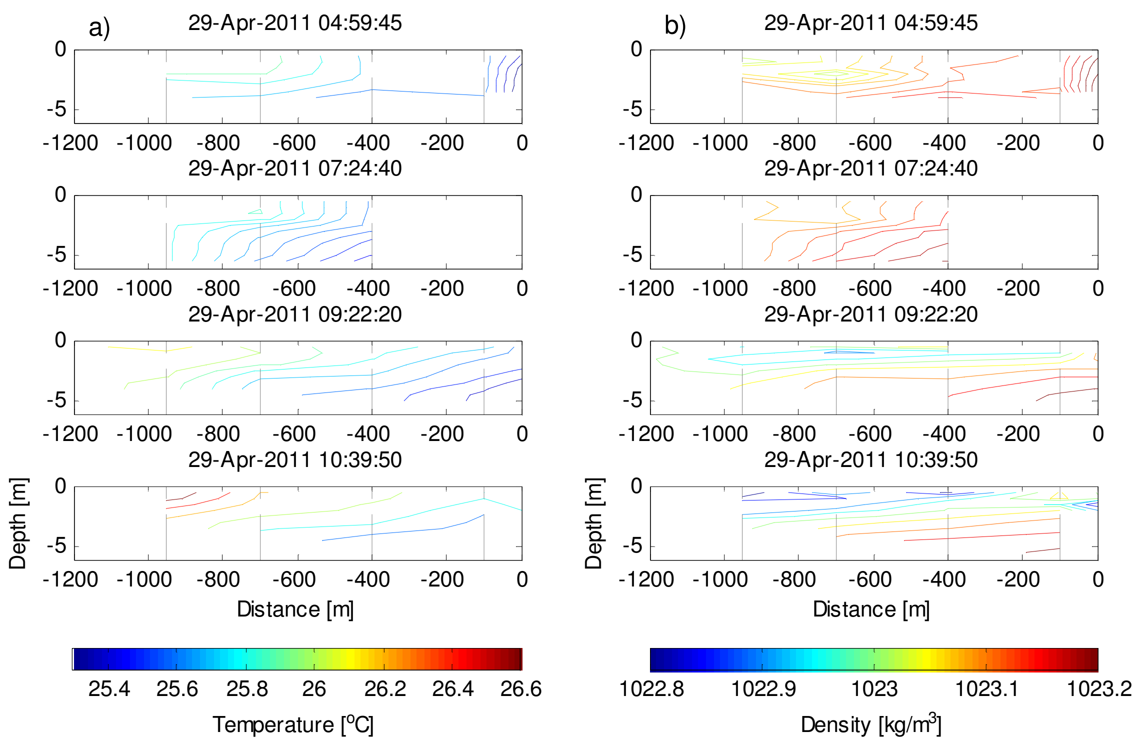

Figure 11. Contour plots of temperature and density in Ala Moana lagoon based on profiles taken at locations indicated by vertical lines.

4. Discussion and Conclusions

Figure 12 shows temperature, salinity and density profiles of all the data taken during the morning experiment on April 29, 2011. This includes all of the REMUS data from Honolulu Harbor to Ala Moana and offshore of Kilo Nalu, temperatures over the reef, surface temperature and salinity in the lagoon, profiles taken around Ala Moana reef, not only in the lagoon but also on the ocean side of the reef, and bottom and surface measurements at Kilo Nalu. From these plots it is seen that, offshore and at greater depths, temperature and salinity vary only marginally. In contrast, the range for measurements made around Ala Moana reef is almost a factor of 10 greater. These results support the observations of thermally driven exchange noted at the Kilo Nalu 12m site by showing a clear thermal gradient between Kilo Nalu and the nearshore area. The generation of cold and warm water, such as is observed at Ala Moana, can drive the cross-shore circulation patterns seen offshore.

Although there were no current meters other than the ADCP at Kilo Nalu, a hypothesis can be made about the flow of water based on the observed water properties. There are two different phases of the thermal exchange mechanism: cooling and heating. As observed at Kilo Nalu, during cooling the coldest water flows offshore at the bottom. There is a compensating onshore flow at the surface with temperatures that are slightly warmer than the bottom but still cold compared to daytime temperatures. This cool water moving onshore will eventually reach the reef where it will quickly be cooled even more over the shallow reef top where the coldest temperatures are observed (Figure 12a, magenta). From the reef top it will either pour into the lagoon or will flow east and west toward the channels. Some of the coldest temperatures were observed in these channels (Figure 12a, blue). Temperatures in the lagoon did not drop as low as the coldest temperatures over the reef, however (Figure 12a, green). There were two other observations that suggest that something different was happening in the middle of the reef. The water mid-reef was not as cold as either end (Figure 4), but REMUS identified a cold spot just offshore of the mid-reef section (Figure 6).

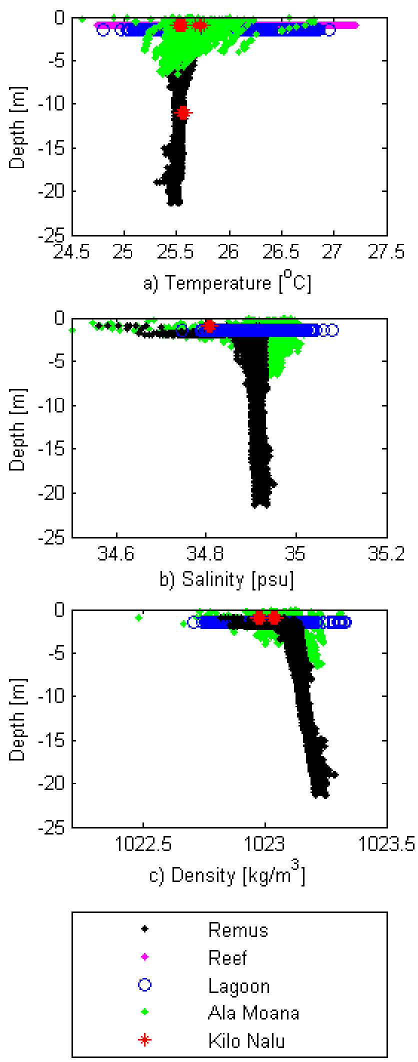

Figure 12. Temperature, salinity, and density profiles using all data collected during the morning of April 29, 2011.

During the heating phase, the exchange profile observed at Kilo Nalu switches directions so that the warmest water is flowing offshore at the surface and cooler offshore water flows onshore at depth. This offshore water flows along the bottom, which is becoming shallower, until it reaches the reef. Wave action at the offshore end of the reef drives an onshore flow over the reef, where water is heated, reaching the highest observed temperatures (Figure 12a, magenta). The heated water flows into the lagoon and toward the ends of the reef, flowing offshore through the channels.

Although it is difficult to fully verify this concept with the available data, this hypothesis provides an idea of the processes occurring and a starting point for future studies. It also highlights the complexity of the system, since there are some observed details that are not yet explained.

The combined observations from this nearshore experiment and from the Kilo Nalu 2010 dataset highlight the importance of thermally driven exchange over tropical fore-reefs. Previous observations from Monismith et al. (2006) identified this mechanism over a reef with steep bottom slope at Eilat, Israel. Now this same mechanism has been identified for a moderate slope on the south shore of Oahu, where wave forcing is important. We have also identified a shallow reef-lagoon system that may be important in driving the thermal exchange. This mechanism should be considered when studying cross-shore currents at locations with similar fore-reef environments.

References

Austin, J.A., S.J. Lentz. 2002. "The Inner Shelf Response to Wind-Driven Upwelling and Downwelling". *Journal of Physical Oceanography*, 32: 2171-2193.

Boden, B.P. 1952. "Natural Conservation of Insular Plankton". *Nature*: 169, 697-699.

Cowen, R.K. and S. Sponaugle. 2009. "Larval Dispersal and Marine Population Connectivity". *Annual Review of Marine Science:* 1, 443-66.

Farrow, D.E. and J.C. Patterson. 1993. "On the response of a reservoir sidearm to diurnal heating and cooling". *Journal of Fluid Mechanics*: 246, 143-161.

Fairall, C.W., E.F. Bradley, D.P. Rogers, J.B. Edson, and G.S. Young. 1996. "Bulk parameterization of air-sea flux for Tropical Ocean-Global Atmosphere Coupled-Ocean Atmosphere Response Experiment". *Journal of Geophysical Research*: 101, 3747-3764.

Fewings, M., S.J. Lentz, J. Fredericks. 2008. "Observations of Cross-Shelf Flow Driven by Cross-Shelf Winds on the Inner Continental Shelf". *Journal of Physical Oceanography*: 38, 2358-78.

Fischer, H.B., E.J. List, R.C.Y. Koh, J. Imberger, N.H. Brooks. 1979. *Mixing in Inland and Coastal Waters.* Academic Press, 483 pp.

Fung, I.Y., D.E. Harrison, and A.A. Lacis, 1984. "On the variability of the net longwave radiation at the ocean surface". *Reviews of Geophysics and Space Physics:* 22, 177-193

Genin A., S.G. Monismith, M.A. Reidenbach, G. Yahel, and J.R. Koseff. 2009. "Intense benthic grazing of phytoplankton in a coral reef". *Limnology and Oceanography*: 54, 938-951.

Hatcher, B.G. 1997. "Coral Reef Ecosystems: how much greater is the whole than the sum of the parts?" *Coral Reefs:* 16, Suppl., S77-S91.

Hench, J.L, J.J. Leichter, S.G. Monismith. 2008. "Episodic circulation and exchange in a wave-driven coral reef and lagoon system". *Limnology and Oceanography:* 53, 2681-2694.

Huyer, A. 1976. "A comparison of upwelling events in two locations: Oregon and Northwest Africa". *Journal of Marine Research*: 34, 531-546.

Kellogg, C.A., J.B. Rose, S.C. Jaing, J.M. Thurmond, J.H. Paul. 1995. "Genetic diversity of related vibriophages isolated from marine environments around Florida and Hawaii, USA". *Marine Ecology Progress Series*: 120, 89-98.

Leichter, J.J., S.R. Wing, S.L. Miller, M.W. Denny. 1996. "Pulsed delivery of subthermocline water to Conch Reef (Florida Keys) by internal tidal bores". *Limnology and Oceanography*: 41, 1490-1501.

Leopold, L. 1948. “Diurnal Weather Patterns on Oahu and Lanai, Hawaii”. *Pacific Science*: 2, 81-95.

Monismith S.G., D.A. Fong. 2004. “A note on the potential transport of scalars and organisms by surface waves”. *Limnology and Oceanography*: 49, 1214-1217.

Monismith, S.G., A. Genin, M.A. Reidenbach, G. Yahel, and J.R. Koseff. 2006. “Thermally Driven Exchanges between a Coral Reef and the Adjoining Ocean”. *Journal of Physical Oceanography*, 36: 1332-1347.

Monismith, S.G., J. Imberger, and M.L. Morison. 1990. “Convective motions in the sidearm of a small reservoir”. *Limnology and Oceanography*: 35, 1676-1702.

Paul, J.H., J.B. Rose, S. C. Jiang, P. London, X. Xhou, and C. Kellogg. 1997. “Coliphage and Indigenous Phage in Mamala Bay, Oahu, Hawaii”. *Applied and Environmental Microbiology*: 63, 133-138.

Pawlak, G., E.H. De Carlo, J.P. Fram, A.B. Hebert, C.S. Jones, B.E. McLaughlin, M.A. McManus, K.S. Millikan, F.J. Sansone, T.P. Stanton, J.R. Wells. 2009. “Development, Deployment, and Operation of Kilo Nalu Nearshore Cabled Observatory”. IEEE OCEANS 2009 Conference, Bremen.

Phillips, O.M. 1966. “On turbulent convection currents and the circulation of the Red Sea”. *Deep Sea Research*: 13, 1149-1160.

Symonds, G. and R. Gardiner-Garden. 1994. “Coastal density currents forced by cooling events”. *Continental Shelf Research*: 14, 143-157.

Tragou, E. and C. Garrett. 1997. “The shallow thermohaline circulation of the Red Sea”. *Deep Sea Research*: 44, 1355-1376.